

DIPLOMARBEIT

3D-PRINTING OF THERAPEUTIC NANO-PARTICLES

ausgeführt zum Zwecke der Erlangung des akademischen Grades einer

Diplom-Ingenieurin

unter der Betreuung von

Ao.Univ.Prof. Dipl.-Ing. Dr. mont. Jürgen Stampfl

am

Institut für Werkstoffwissenschaften und Werkstofftechnologie

Bereich Nichtmetallische Werkstoffe

eingereicht an der Technischen Universität Wien, Fakultät für

Maschinenwesen und Betriebswissenschaften

von

Sonja Baumgartner, B.Sc.

Matrikelnummer 0925792

Hohe Wand-Straße 13/3, 2344 Maria Enzersdorf

ABSTRACT

Two-photon polymerization (2PP) is a novel CAD/CAM-based 3D printing technology, allowing the fabrication of complex structures with sub-micron lateral resolution. Due to the small achievable size of the parts, many possible applications in different fields have been demonstrated. The 2PP technique provides the possibility of producing a large number of structures with high speed and accuracy at the same time. Such custom-made parts containing features at the nanoscale in combination with biocompatible hybrid materials make this additive manufacturing technology particularly attractive for biomedical applications.

In the first part of this work, investigations on the influence of the material composition on the resolution of the structures are presented. 2PP processing of different photosensitive sol-gel materials on the basis of zirconium, tantalum and titanium with variable inorganic content was tested. The printing is performed with variable power and writing speed as well as different structure design. Furthermore the influence of volumetric pixel (voxel) size as well as the direction of hatching is investigated. The observed deviation between the lateral and axial resolution is implemented in the structures' geometry.

Finally, investigations of the interaction between the various structures and different cell lines are presented. It can be shown that the cells tend to collect the particles and take them in.

KURZFASSUNG

Zwei-Photonen-Polymerisation (2PP) ist eine neuartige CAD/CAM-basierte 3D-Druck Technologie. Sie erlaubt die Herstellung von komplexen Strukturen mit einer Auflösung im Mikro- bis Nanometer Bereich. Da sehr geringe Werkstückgrößen realisiert werden können, sind die Anwendungsbereiche sehr breit gefächert. 2PP ermöglicht die Produktion von hohen Stückzahlen mit gleichzeitig großer Geschwindigkeit und Genauigkeit. Neue biokompatible Materialien und die Möglichkeit der Herstellung benutzerdefinierter Strukturen, macht diese Technologie besonders attraktiv für biomedizinische Anwendungen.

Im ersten Teil dieser Arbeit wird der Einfluss der Materialien und derer Zusammensetzungen auf die Auflösung der Strukturen untersucht. Es werden unterschiedliche Sol-Gel Materialien auf Basis von Zirkonium, Tantal und Titanium getestet. Der Druck wird mit variabler Leistung, Schreibgeschwindigkeit und verschiedensten Strukturen durchgeführt. Außerdem wird der Einfluss der Voxel-Größe (volumetric pixel) und der Hatch Einstellungen untersucht. Die unterschiedliche Auflösung in lateraler und axialer Richtung wird ebenfalls berücksichtigt und in das Strukturdesign mit einbezogen.

Der letzte Teil dieser Arbeit widmet sich der Untersuchung des Einflusses von Partikeln auf Zellen. Es kann gezeigt werden, dass die verwendeten Zellen die Tendenz haben, die Partikel aufzusammeln.

ACKNOWLEDGEMENTS

I would like to use this opportunity to express my gratitude to those who supported me during my studies and especially during this thesis.

First of all I would like to thank my supervisor ao. Prof. DI Dr. Jürgen Stampfl for giving me the opportunity to work in this interesting field and get to know more about this new manufacturing technology.

Secondly, I would like to thank Dr. Aleks Ovsianikov who would share his great knowledge about two-photon polymerization and cell related topics whenever needed.

My special thanks go to DI Peter Gruber for his great support from the very start. His knowledge about the 2PP-system and the physical and mechanical background not only was great help during this work but saved me from desperation more than once.

Last but not least I want to thank the Institute of Material Science staff, especially my colleagues. Whenever it was needed, someone was there to help. It is a pleasure to work with them and makes me looking forward to future cooperation.

I also want to thank my friends and family for their encouragement and support in any way.

CONTENTS

Abstract.....	<i>i</i>
Kurzfassung	<i>ii</i>
Acknowledgements	<i>iii</i>
1 Introduction.....	1
2 Theoretical Background	3
2.1 Polymerization	3
2.1.1 Photopolymerization	4
2.2 Photosensitive Materials	5
2.2.1 Sol-Gel process	5
2.3 One-photon absorption	6
2.4 Two-photon Absorption	6
2.5 Two-Photon Polymerization	8
2.6 Microscopy.....	9
2.6.1 LSCM – Confocal Laser Scanning Microscopy.....	9
2.6.2 SEM – Scanning Electron Microscope.....	12
3 Experimental setup and materials	13
3. 1 2PP System	13
3. 2 Femtosecond laser.....	13
3.3 AOM.....	14
3.4 Galvometer-Scanner.....	14
3.5 Stage	14
3.6 Objective	15
3.7 CMOS-Camera	16
3.8 Materials	17
4 Methods of fabrication of micro- to nanoscale particles	20
4.1 Sample Preparation	21
4.2 Developing Procedure	22
4.3 Structuring Parameters.....	23
4.3.1 Writing Speed	23
4.3.2 Power.....	24
4.3.3 Hatch and dZ.....	25

4.3.4 Delays	25
4.4 Cell Counting	26
4.5 Cell preparation.....	27
4.5.1 Staining 1 – Live/Dead stain	27
4.5.2 Staining 2 – F-actin stain.....	28
5 Results and discussion.....	29
5.1 Preparation	29
5.2 Building Speed.....	33
5.3 Power.....	34
5.4 Polymerization threshold	37
5.5 Layout and hatching	39
5.5 Freestanding particles	42
5.5.1 Parameter	42
5.5.2 LSM-images	46
5.5.3 Storage.....	47
5.6 In vitro studies	48
5.6.1 Cytotoxicity.....	48
5.6.2 Staining 1	49
5.6.3 Staining 2	51
6 Conclusion	56
7 Bibliography	58
8 Table of figures	60
9 List of tables	62

1 INTRODUCTION

Additive manufacturing is any process of making three-dimensional objects by a layer-by-layer combination of voxels (volumetric pixels) [26]. Originally those technologies were used to produce prototypes which led to the term “Rapid prototyping”. Due to constant enhancements in this manufacturing field concerning applicable materials and production equipment, it became more and more interesting for commercial applications. It was then divided into “Rapid manufacturing” and “Rapid prototyping”. This is, however, an unfavourable description since “rapid” is a relative parameter and speed varies greatly in the different manufacturing technologies. Generally the process chain can be separated into four steps:

- *3D-data*: A 3D-model of the part has to be generated. This is normally done in a CAD-program and then exported as .stl-file. In data format .stl, a surface model is generated of a triangular mesh.
- *Slicing*: The solid model is divided into layers of usually constant thickness by a software
- *Printing*: Those layers are assembled in a manufacturing facility to form the part to be produced
- *Linking*: If the layers are not automatically linked during structuring, this is done afterwards (e.g. sintering).

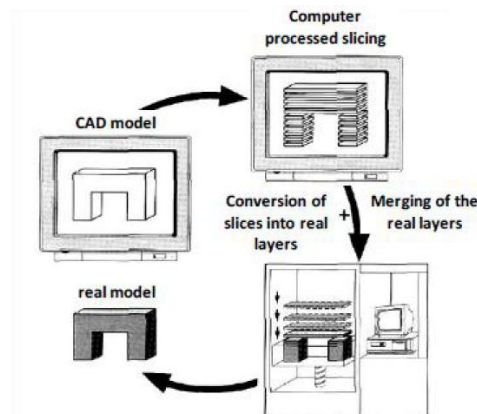


Figure 1 Process chain of an additive manufacturing technology

Nearly all additive manufacturing processes somehow share those steps. A relatively new approach to 3D-structuring is two-photon polymerization (2PP). 2PP, like one-photon polymerization, bases upon controlled triggering of chemical reactions. Those processes are called photon absorption and date back to discovering from before 100 years. Now, with the technological potential of ultra-

short-pulsed lasers and high resolution optical devices, 2PP is an upcoming manufacturing technology.

2PP does not only provide the possibility of producing structures with a size down to $65\mu\text{m}$ [8] but also a very high amount of fabricates in short time and with high accuracy. Due to miniature size of the structures, a wide field of applications can be demonstrated. So far, 3D optical data storage, optical tweezers, fluorescence microscopy, 2D and 3D micro-fabrication are only a few amongst other uses for 2PP.

In combination with new biocompatible materials, 2PP becomes interesting for biomedical applications. For those, new hybrid photosensitive sol-gel materials consisting of organic and inorganic complexes are very promising. Different compositions and photoinitiator concentrations can be easily realized and adapted for each particular use. Those new materials allow structuring at a nanoscale level with high resolution.

Cell culture is a new field of application for the 2PP-produced nano-particles. Particle uptake for example in favour of transfection is only one possibility to think of.

2 THEORETICAL BACKGROUND

2.1 POLYMERIZATION

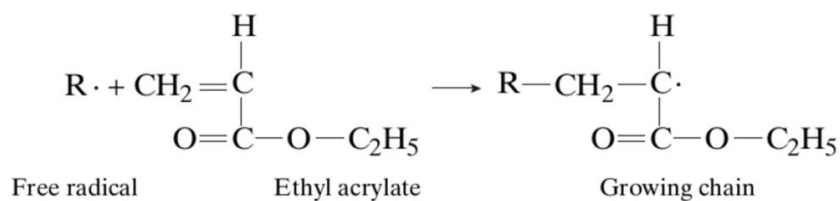
Polymerization is a collective name for chemical synthesis of forming polymer chains or three-dimensional networks of reacting monomer molecules. [1] Although there are many forms of polymerization and systems to categorize them, it can basically be differentiated between step-growth and chain-growth polymerization. Where step-growth polymerization results from condensation and addition polymerization, chain-growth polymerization involves linking up of molecules.

Condensation polymerization describes the process of joining two molecules which lose a small molecule as by-product where they are linked. In contrast, addition polymers are formed by addition polymerization where monomers are linked together without the loss of any molecule or atom.

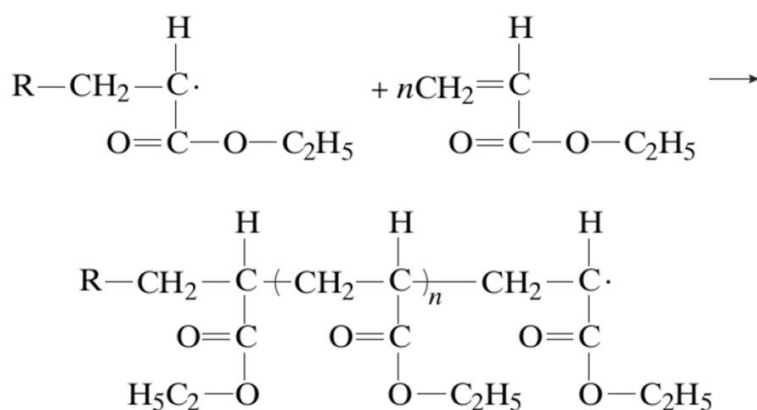
Chain growth polymerization can be classified into radical, cationic, anionic and coordination polymerization. For two-photon polymerization (2PP), free radical polymerisation is by far the most important. It can be divided into the following steps:

- chain initiation
- chain propagation
- chain termination

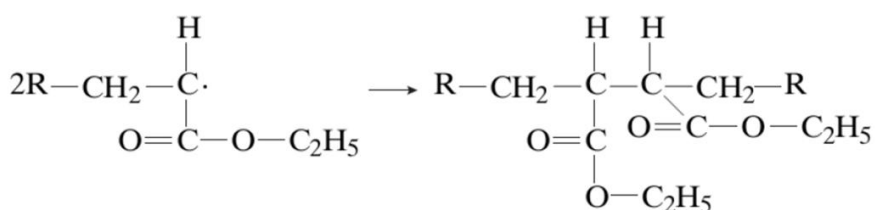
For getting the polymerization started an initiator is needed. Initiation is happening when radicals ($R\cdot$ in figure 2) of this initiator react with the monomer. By breaking the double bond of the monomer a free radical is created. During the chain propagation monomers start attaching to this free radical. This happens in the part of a second and goes on until chain termination is induced. Chain termination can occur either through combination or disproportionation. Combination occurs when two free radicals happen to react (figure 2c), which then leads to a non-reactive chain, while disproportionation takes part when an atom is transferred from one chain to another. This then results in two polymeric chains.



(a) Initiation



(b) Propagation



(c) Termination

Figure 2 (a) A free radical is formed and reacts with the monomer. (b) Those monomer molecules combine to large, fast growing chains. (c) Termination through combination: Two radicals combine and propagation is stopped. [3]

2.1.1 PHOTOPOLYMERIZATION

In case of photopolymerization, a so called photoinitiator (PI) is needed. Like all, those initiators need a certain energy to form radicals. For photoinitiators this energy is provided by photons. Depending on the application, the light source may be for example an UV-lamp in case of one-photon absorption or curing resins, a laser beam for multi-photon absorption or a visible light source. Since the energy provided by a photon cannot be easily quantified, the optimal wavelength for the PI has to be found. This is done by plotting the sensitivity over the wavelength and therefore finding the peak sensitivity of the PI.

2.2 PHOTSENSITIVE MATERIALS

Polymers that change their properties when exposed to light are called photopolymers. They consist of monomers, a photoinitiator and usually some additives to regulate the properties. Photopolymers are the material of choice when working with 2PP. However, each component of the formulation has different influences. One of the most important properties of a photopolymer is the viscosity of its monomer. When the viscosity of the resin is too low, the structures float when not having contact to the substrate. Even structuring itself may become problematic since the layers are eventually shifting against each other due to the motion of the stage. Another important component is the photoinitiator. Although basically every initiator which is used for 1PP (UV-photoinitiators) can be used for 2PP, their 2PP cross section is relatively low which then requires high intensity to work properly. The advantage of using photoinitiators especially designed for 2PP is therefore the lower intensity needed and furthermore a higher speed.

Depending on the application for which the photopolymer is used – e.g. for biological use – it may also fulfil other requirements like toxicity or biodegradability. The photoinitiator further influences the colour of the material, which may also be respected.

2.2.1 SOL-GEL PROCESS

In the sol-gel process solid materials are produced from small molecules. It involves the transformation of a liquid solution (*sol*) into an integrated network of particles or polymers (*gel*). The sol-gel process is quite flexible; even composites with considerably different properties such as organic - inorganic formations can be made. The material is generally formed through four steps:

- *(catalytic) hydrolysis and condensation:* Precursors or monomers (metal oxides or metal alkoxides) are mixed with water and undergo hydrolysis and condensation; a porous interconnected cluster structure is formed. As catalyst an acid like HCl or a base such as NH₃ can be employed.
- *gelation:* The solvent is removed and a gel is formed. This happens by heating at low temperature. In this step significant volume loss occurs.
- *polymerization:* Because of double bonds and at the presence of a photoinitiator, photoinduced radicals cause polymerization only where they are present. In this step no volume loss occurs
- *development:* The sol-gel is immersed in a solvent and non-polymerized material is removed.

2.3 ONE-PHOTON ABSORPTION

In case of one-photon absorption (single-photon absorption or 1PA) polymerization is initiated by a single photon. This way of inducing photo polymerization is therefore called one-photon polymerization (1PP). The absorption does not only take place in the focal point but all along the laser beam path. Therefore fabrication of a structure is not possible inside the formulation but limited to its surface.

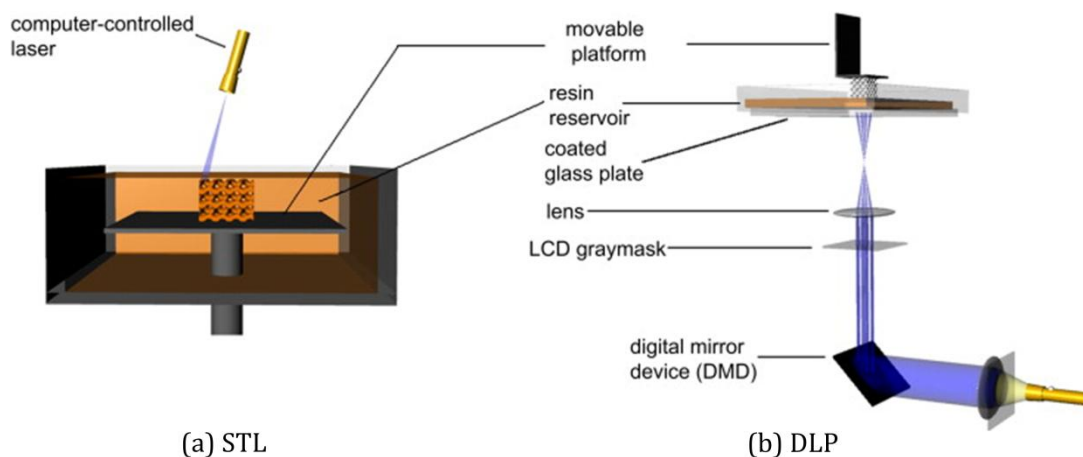


Figure 3 Schemes of two different additive manufacturing technologies; (a) Stereolithography apparatus (SLA); a bottom-up system with scanning laser; (b) a top-down setup with digital light projection (DLP) modified from [4]

There are two different additive manufacturing technologies which use light polymerization (figure 3). The first one is stereolithography (SLA), shown in figure 3a. STL employs a liquid photopolymer and an ultraviolet laser to cure line-by-line of each layer of the model by tracing the laser beam on the surface of the resin. After one layer is finished, the platform descends, the part is re-coated with fresh material and the next patterns are traced by the UV-laser. When printing is done the parts are then cleaned of the excess material and cured in an UV oven. Digital light processing (DLP) is the second technology. In contrast to STL it uses an incoherent light source and a digital micro-mirror device to cure one layer at once like shown in figure 3b.

2.4 TWO-PHOTON ABSORPTION

Firstly described by Göppert-Mayer in 1931 [5], multi-photon absorption (MPA) is a process of exciting a molecule to an energy electronic state by combination of multiple photons. This results in an energy state higher than that reachable for one-photon absorption. Due to very high photon intensities required for this process it could not be proven experimentally at that time since former light sources were not suitable. With the advent of the laser, Kaiser and Garret [6] were then able to demonstrate two-photon absorption (TPA) in the year 1961. For MPA to work, two or more photons must be present simultaneously in order to impart enough energy for the transition. The simplest version of MPA is the two-photon absorption (TPA)

or 2PA). In TPA two photons of about the same energy interact with a molecule and produce an energy state equivalent to the excitation of a single photon of twice the energy. [13]

$$\Delta E = h \cdot \nu_{IR1} + h \cdot \nu_{IR2} \quad (1)$$

Formula 1 can be used to describe the TPA process. The dashed line in figure 4 represents the so called virtual state. This very short-lived virtual state is occupied when the first photon $h\nu_1$ is absorbed. If the second photon $h\nu_2$ is absorbed within the short time of about 1femtosecond (fs) the excited state S_1 can be reached. Hence, ultrafast (femtosecond pulsed) lasers are usually used to drive TPA.

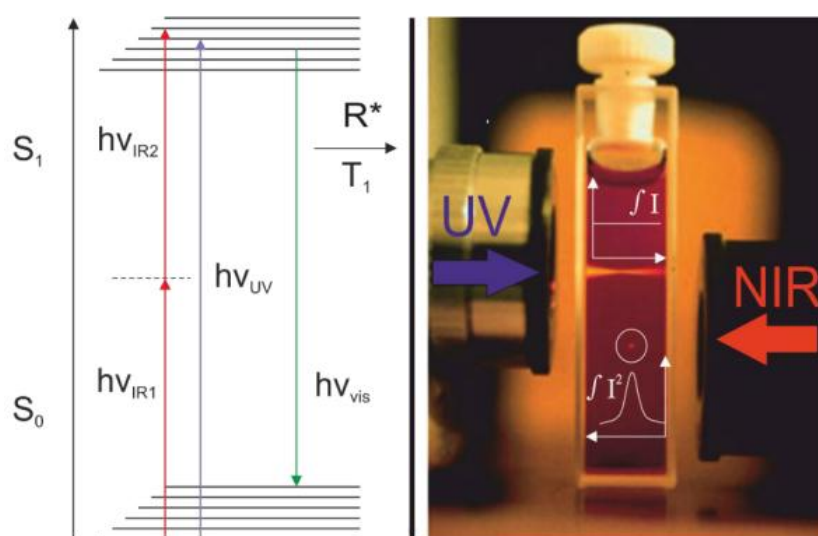


Figure 4 Left picture: Jablonski diagram; $h\nu_{IR1}$ and $h\nu_{IR2}$: first and second photon absorbed in NIR spectral range; $h\nu_{UV}$: photon in UV spectral range; $h\nu_{vis}$: photon emitted in visible range; R^* : radical; T_1 : Triplet state; Right picture: Example of one- and two-photon excitation of fluorescence. [10]

The rate of absorption in the sample depends on the product of the laser intensity and the number of molecules in the cross section of the laser beam. For one-photon absorption the number of excited molecules along the transverse plane of the laser beam is constant. Therefore no fluorescence can be localized in the focal area (figure 4). In opposite the rate of absorption in TPA is proportional to the square of the intensity. In the focus point of the laser the density of excited molecules is the highest while in any other plane of the sample the intensity is not high enough to cause TPA [13].

Since the probability of absorption is a function of the power of the intensity, MPA is often referred to as nonlinear absorption. With currently available femtosecond lasers, MPA becomes more and more commercially attractive. Applications where the principle of MPA is used are for example fluorescence microscopy, optical tweezers, fs-laser surgery as well as 2D and 3D micro-fabrication. [10]

2.5 TWO-PHOTON POLYMERIZATION

Additive manufacturing or 3D printing is a technology to create three dimensional objects. Two-photon polymerization (2PP) is one of those additive manufacturing technologies (AMT). 2PP is based on the principle of TPA. While for STL the fabrication is limited to the surface of the formulation (figure 5b), with 2PP the structure can be directly written inside the material (figure 5a).

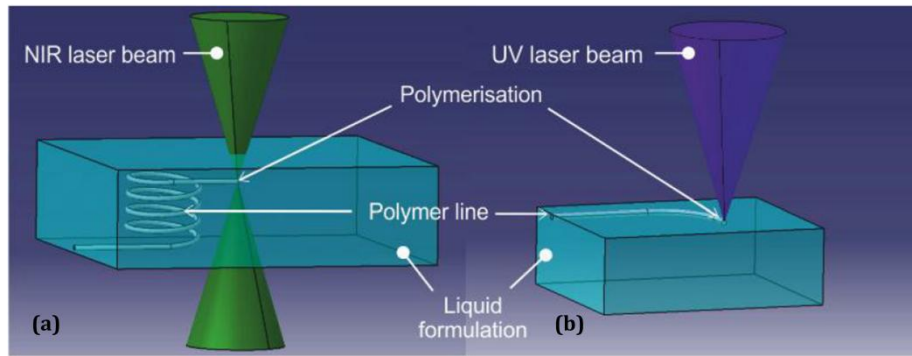


Figure 5 (a) Polymerization takes part inside the material since 2PP is only limited to the focal point of the microscope, (b) 1PP/STL is limited to the surface of the material and therefore requires a layer-by-layer printing [19]

Due to the nonlinearity of TPA the size of the polymerized volume in the focal point (volumetric pixel or voxel) can be reduced below the diffraction limit and a resolution of down to 65nm [8] can be achieved. Depending on the laser intensity the voxel-size varies (figure 6).

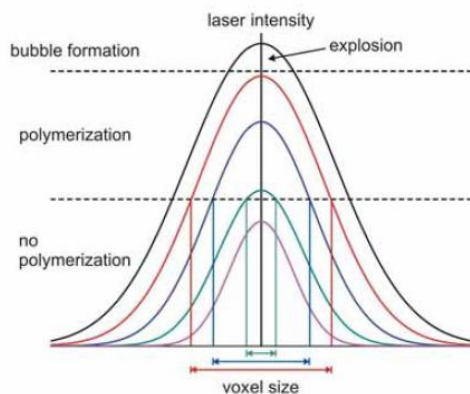


Figure 6 Dependence of the polymerized volume on the laser intensity in 2PP with the polymerization threshold and the threshold for polymer destruction [2]

Therefore there are two threshold values for two-photon polymerization. When the first one is reached, the polymerization is initiated. Passing the second one leads to destruction of the material. Since a certain energy level has to be exceeded for the photoinitiator to produce radicals, below the first polymerization threshold no lasting structure can be produced. However, if this critical value is only slightly transcended the smallest possible voxel-size might be achieved. This is only

theoretical though, since too little power results in dissolving of the structure at the latest during developing. Furthermore the resolution is also limited by the stability of the laser as well as the setup of the 2PP-system. Too much power, however, leads to damaging by burning or bubble formation. This is in fact disastrous since surrounding structures are irreversibly destroyed, too (see also figure 25).

The former drawback of 2PP compared to 1PP was the writing speed of less than 100µm/s while 1PP achieved writing speeds of 1-2000 mm/s [2]. This has changed dramatically though. Modern 2PP-systems like the one used in this thesis reach a maximum marking speed of for example up to 1000 mm/s with a 10x microscope objective [7], which is impossible for one-photon polymerization applications.

In contrast to other 3D-fabrication schemes, two-photon photopolymerization has several advantages:

- 3D structures can be produced inside the material which leads to structures with spatial resolution without being bound to the layer-by-layer approach. In addition the long wavelength used for TPA results in deep penetration of the light. Furthermore the use of femtosecond pulsed laser beams allows to start the desired nonlinear processes at low average power which lowers the probability of thermally damaging the samples
- Like laser scanning microscopes the 2PP-system does not require vacuum condition for operation. It is therefore relatively easy to operate.
- Computer designed models can be directly converted into physical structures. No stamp, mask or mold is needed for fabrication, allowing rapid modifying of designs.

2.6 MICROSCOPY

2.6.1 LSCM – CONFOCAL LASER SCANNING MICROSCOPY

Confocal laser scanning microscopy (CLSM or LSCM) is a technique to get optical images with high resolution and depth of focus. It provides a procedure for non-invasive and direct observation of even thick and living samples. A key feature is the so called optical sectioning process which allows to produce images of focal planes inside a sample. Those planes are then reconstructed by a computer. With this it is possible to get a three-dimensional reconstruction of the sample, independent of its topology. This is useful especially for opaque samples since it allows getting a look inside the structures to a certain degree. Whereas conventional microscopes can see as far as the light can penetrate into the sample, the confocal microscope only shows one focal plane at a time. Therefore a high depth of focus can be achieved.

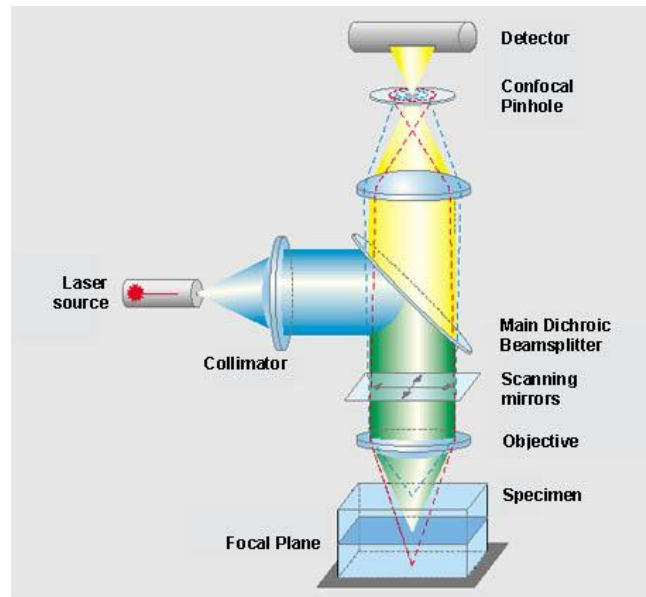


Figure 7 LSCM beam path

Figure 7 shows the principal setup of an LSCM. The light source is a laser beam which passes through an aperture and is then focused by an objective lens into or on the sample. For this microscopy to work, the specimen has to be fluorescent. The reflected and scattered laser light as well as the fluorescent light from the illuminated sample is then passed back through the lens, separated by a beam splitter and sent to a detection apparatus. With the original excitation wavelength blocked, the fluorescent wavelengths pass a pinhole. Afterwards the light signal is transformed into an electrical signal which is then recorded by a computer.

The set of those images obtained at various depths within the specimen is called *z stack*. For getting a 3D-reconstruction as close to reality as possible, at first the correction factor has to be defined (see below). Without correcting, the images would then experience a distortion caused by the usage of false refractive indices. Next step is then to set the first and last slice to define the area of scanning. At last, the numbers of slices can be determined. This has a great impact on the resolution of the final image. The more layers are scanned, the less distance is between them and the more information the program has to reconstruct the structure.

Furthermore, the laser power and pinhole diameter have to be set. In order to not get an overexposed image, the laser power should be held low. The pinhole diameter is defined by so called Airy units (AU). If it is for example set to 1 AU, only the first order diffraction pattern passes through the aperture. The size of the scanning volume and therefore the resolution of conventional optical microscopes is defined by the spot size which should be close to the diffraction limit to get optimal results. This on the other hand is determined by the numerical aperture of the objective lens and laser wavelength used. By closing down the confocal aperture, the

other (higher) orders are blocked which results in a higher resolution but slightly decrease of brightness. [5]

In the program used for imaging in this thesis (ZEN, Carl Zeiss software) it is further possible to increase the digital gain in order to get brighter images.

The biggest advantage of using LSCM compared to the scanning electron microscope is the possibility of non-invasive observations of living cells and liquid or humid samples. Although confocal laser microscopy requires a minimum of sample preparation, living specimens often have to be treated with special dyes in order to make them fluorescent.

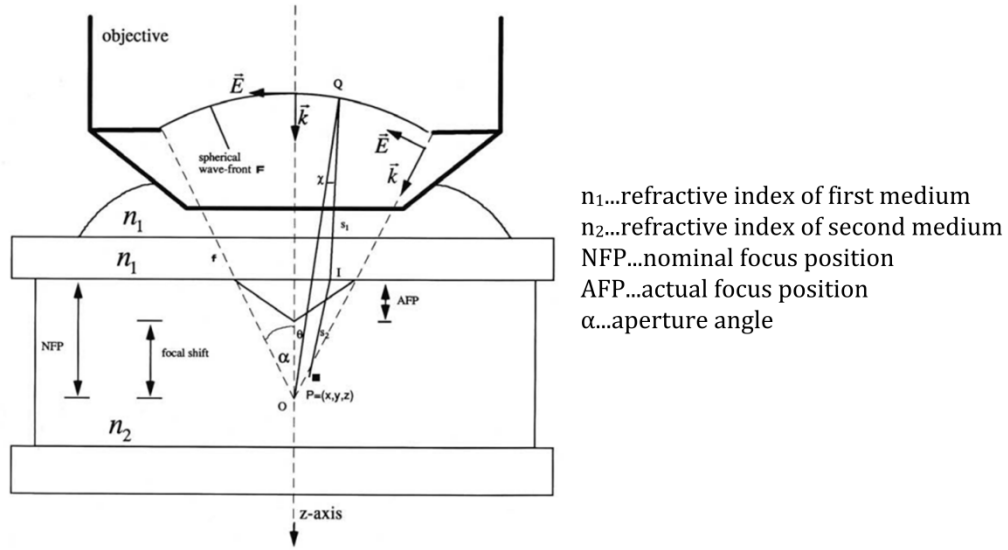


Figure 8 High NA microscope objective [6]

Figure 8 shows a standard situation encountered in LSCM. When using an immersion liquid of correct refractive index, aberrations can be neglected. However, most specimens have a different refractive index (n_1) than that of the cover glass/immersion liquid (n_2). At the interface between cover glass and specimen the light is partly reflected and partly refracted and therefore undergoes changes in phase and amplitude. This results in aberrations. Therefore it is necessary to distinguish between two focus positions: the nominal focus position (NFP) and the actual focus position (AFP). While NFP is the distance between the interface and the focus point under unaberrated circumstances, AFP indicates the distance between cover glass and focal point when aberrations occur. NFP is given by formula (2), where α_1 is the aperture angle and α_2 the refracted angle. NA is the numerical aperture of the microscope objective. For low numerical aperture objectives formula (2) can be simplified to (3). [6]

$$NFP = \frac{\tan \alpha_1}{\tan \alpha_2} AFP = \frac{\tan [\sin^{-1}(\frac{NA}{n_1})]}{\tan [\sin^{-1}(\frac{NA}{n_2})]} AFP \quad (2)$$

$$NFP = \frac{n_1}{n_2} AFP \quad (3)$$

The Refractive Index Correction input box in ZEN allows to consider the different refractive indices between the immersion medium of the objective (n_1) and the embedding medium of the specimen (n_2), which can be set between 0.5 and 3. The number should correspond to the ratio $r = n_1 / n_2$.

For better depth of focus, thiodiethyenglycol is put on the samples. With a refractive index of 1.518 – which is the same as glass – a much higher resolution can be achieved.

2.6.2 SEM – SCANNING ELECTRON MICROSCOPE

Scanning electron microscopy uses a focused beam of electrons to scan a sample. By interaction of the specimen's atoms with the electrons, various signals are produced which can then be detected and analysed by a computer. There are several detectors available for SEM, but it is unusual that a single machine is equipped with all. However, all SEMs are by default equipped with secondary electron detectors (SE) which allow to reveal details of down to 0.4 nm [6]. Also, it is possible to get a high-resolution 3D appearance due to a large depth of field (DOF).

Nonconductive samples have to be coated to make them electrically conductive. Since they tend to charge when getting in contact with the electron beam, the samples have to be electrically grounded. This charging usually results in scanning faults and image artefacts with reduce the resolution significantly. Coating of the samples in this thesis is done by sputtering with gold in low-vacuum.

The critical part of scanning electron microscopy is the need of drying the samples. Therefore this microscopy technique may not be suitable for some specimens and generally requires more sample preparation.

Due to a high surface tension when vaporizing propanol or even water, the more filigree structures are destroyed. Therefore hexamethyldisilazane (HMDS $C_6H_{19}NSi$) is applied before drying. HMDS lowers the surface tension and leads to weaker capillary forces during the evaporation [25]. However, even drying with HMDS has to be done with caution and cannot always completely prevent destruction.

3 EXPERIMENTAL SETUP AND MATERIALS

3.1 2PP SYSTEM

The 2PP-system used was developed and built by Peter Gruber in the context of his thesis [7]. Figure 9 shows the basic setup of the 2PP-system.

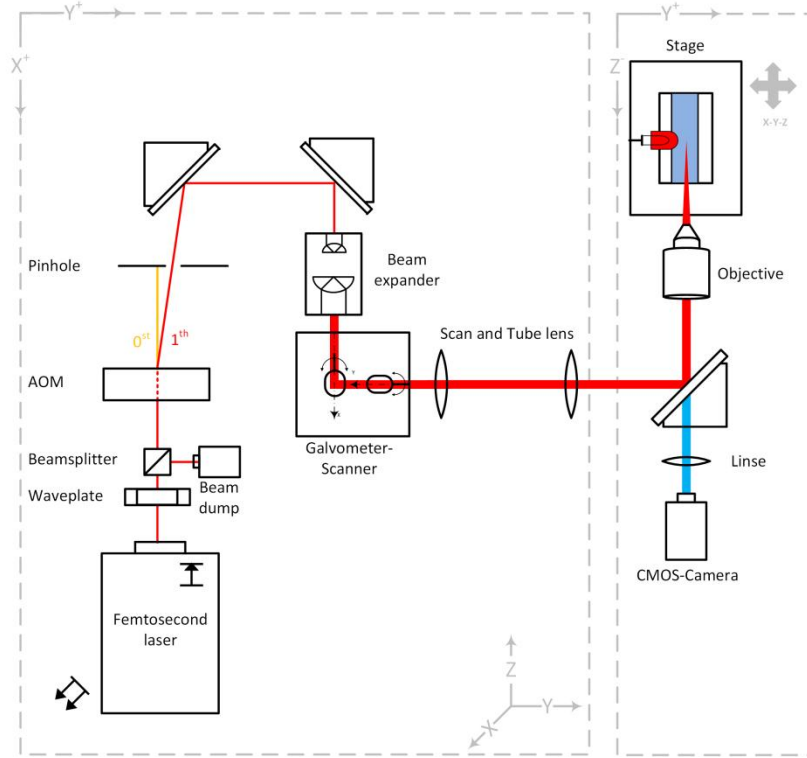


Figure 9 2PP-system [18]

The femtosecond pulsed beam of the Ti:Sapphire laser passes through a beam splitter and afterwards through an acousto-optic-modulator (AOM). The AOM functions as both, power modulator and shutter. In order to adjust the laser beam power properly, it is necessary to only let the first order diffraction pass the pinhole which is given here. In this setup the laser beam power can be regulated between 0 and 500mW. Before leading the beam into the galvo-scanner it has to pass through the beam expander in order to overfill the back aperture of the objective and therefore get a small focal point. An oil-immersion objective then leads to a movable stage where the sample is mounted. An integrated CMOS-camera prepares live images while structuring.

3.2 FEMTOSECOND LASER

In this setup, the laser source used is a diode-pumped solid state femtosecond Ti:Sapphire laser (MaiTai eHP DeepSe). The laser beam has an average power of 2,9W and is therefore a class 4 laser. However, a beam splitter after the laser

reduces the power to below 500mW (Class 3). The wavelength can be tuned from 690 to 1040nm but is only used at 800nm for this thesis where the peak power of 425kW can be achieved. The typical pulse width of this laser source is 70 fs and the repetition rate is 80MHz. Furthermore the MaiTai has an integrated pulse compressor to ensure the pulse width of 70fs. Cooled down by an external chiller and the space cooling, the operation temperature was kept constantly at around 20-25°C. To have constant working conditions, it also has to be ensured that there is no temperature variation of more than 2°C/h.

Due to a larger focal point a higher laser output power is needed to get the same quality of structures under the same conditions when using a lower numerical aperture (NA) microscope objective. Since a high numerical aperture objective (ZEISS Plan-Apochromat 100x/1.4 immersion oil) is used for the structures in this thesis the peak power of the laser is sufficient. Although with this objective the writing speed is limited by the desired quality of the structures at around 75 mm/s, it would be possible to reach at least 500 mm/s thanks to the stage/scanner combination.

3.3 AOM

In this setup, the AOM (MT110+MDS1C, AA-Optoelectronic) operates as a power modulator and a fast switch. It is slightly tilted to maximize the diffraction efficiency. The light propagates through a transparent crystal where a transducer generates an acoustic wave (100MHz). The zero order diffraction is blocked by a pinhole. By controlling the amplitude of the acoustic wave, the intensity of the first order can be set. The output power has to be fitted since it is not linear.

3.4 GALVOMETER-SCANNER

The galvometer-scanner (intelliSCAN 10, Scanlab AG) deflects the laser beam in XY direction by using two mirrors. Although the field of view (FOV) of the objective is limiting the scanner's writing field, this combination of galvo-scanner and stage allows the production of bigger structures. Also a high marking speed and accuracy can be reached.

3.5 STAGE

As written before, the galvometer-scanner only allows a very small structuring area. For getting bigger structures or writing arrays it is therefore required to additionally move the sample in XY-direction.

The specimen stage in this setup consists of a linear positioning stage (Scanningtisch SCAN^{plus} IM 120x80, Märzhäuser Wetzlar) which moves the sample in X- and Y-direction. For obtaining 3D structures it is necessary to also adjust the position of

the sample in Z, since the focal point of the laser beam is fixed in this direction. This movement is performed by another linear positioning stage.

Both stages are moved by piezo motors with a maximum speed of 250 mm/s and an acceleration of 10mm/s². Since the accuracy of motor and stage is only 1µm, the stages are provided with a linear encoder (LIA-20, “Numerik Jena”). This feedback allows compensating the positioning error of the stage and galvo-scanner.

3.6 OBJECTIVE

The objective defines achievable resolution and size as well as the mark speed threshold of the desired structures. To get a better focus, the laser beam has first to be expanded and then again focused for which a beam expander is applied. In order to get the smallest possible focal spot size the back focal plane of the objective must be filled.

The magnification factor M which defines the minimal distance between two written lines is then - combined with the galvo-scanner - crucial for the final resolution and writing speed. Typically a higher magnification factor is needed for a better spatial resolution of the system. Furthermore the working distance d_w and the numerical aperture NA are major properties of the microscope objectives used for 2PP. As written before, normally two lines can be placed closer together when having a higher magnification. However, if those lines are getting too thick they would start merging when getting too close. To prevent this, the numerical aperture (NA) as a function of the minimal distance d_{min} between two distinguishable structures comes for use. For objectives the NA defines the minimal size of the producible light spot in its focus and is therefore limiting the resolution.

$$NA = n \cdot \sin(\alpha) \quad (4)$$

Where n is the refractive index of the medium between the lens and the observed object (ranges from 1.00 for air, 1.33 for water to 1.51 for immersion oil) [22] and Alpha is half the angular aperture. For air (n=1) the theoretical highest NA is 1 (sin(90°)=1), in practice, however, it is often less. For obtaining higher NAs n has to be increased which can be accomplished by using immersion medium such as water, glycerin or oil.

According to the Rayleigh criterion the lateral resolution for one-photon absorption is [7]:

$$d_{min} = 0,61 \cdot \frac{\lambda}{NA} \quad (5)$$

Since two-photon polymerization (and other multi-photon excitations) is a non linear process, the achievable resolution can be improved:

$$R_{lateral} = 2 \cdot \ln(2) \cdot \frac{0.325 \cdot \lambda}{\sqrt{2} \cdot (NA)^{0.91}} \quad (6)$$

$$R_{lateral} = 2 \cdot \ln(2) \cdot \frac{0.325 \cdot 800}{\sqrt{2} \cdot (1.4)^{0.91}} \approx 188 \text{ nm} \quad (7)$$

$$R_{axial} = \frac{0.532 \cdot \lambda}{\sqrt{2}} \cdot \left(\frac{1}{n - \sqrt{n^2 - (NA)^2}} \right) \quad (8)$$

In this setup a 100x/1.4 immersion oil objective (Carl Zeiss GmbH, Objektive Plan-Apochromat 100x/1.4 Oil M27) is used. By using oil immersion the NA is increased to >1 which reduces the size of the focal point significantly. It can therefore be referred to as high numerical aperture objective.

3.7 CMOS-CAMERA

In order to monitor the position of the focal point and later the structuring process, a CMOS-Camera (UI-3360CP-M-GL, IDS Imaging Development Systems GmbH) is applied after the galvo-scanner behind the first dielectric mirror, which is transparent for visible light. Therefore a red LED ($\approx 620\text{nm}$) can be used to illuminate the sample.

3.8 MATERIALS

For structuring, seven different hybrid materials were used. Those sol-gel materials use zirconium, tantalum and titanium as precursors. All of those hybrids were provided with different amounts of MAAH (in case of Zr and Ta) or ACAC (for Ti). The following tables summarize the composition of the utilized formulations.

Tab. 1 Sol-gel materials

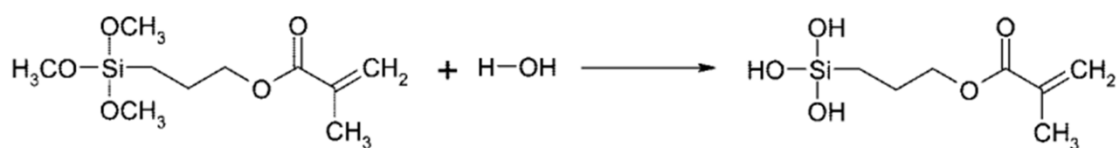
(all numbers in gram)

Zirconium	SOL A	SOL B	SOL C
MAPTMS	5	5	5
ZPO	2,356	2,356	2,356
MAAH	0,438	0,219	0,109
H₂O/HNO₃	0,267	0,267	0,267
H₂O	0,4002	0,4002	0,4002
Total Weight	8,461	8,242	8,132

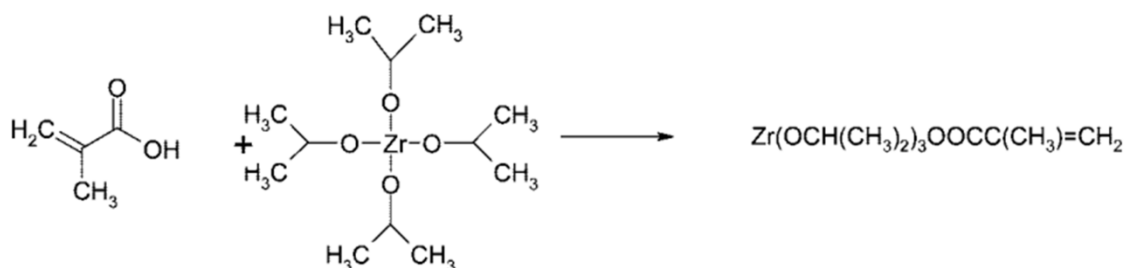
Tantalum	SOL D	SOL E
MAPTMS	5	5
TAO	2,046	2,046
MAAH	0,438	0,109
H₂O/HNO₃	0,267	0,267
H₂O	0,4002	0,4002
Total Weight	8,1503	7,8222

Titanium	SOL F	SOL G
MAPTMS	5	5
TiOP	1,458	1,458
ACAC	0,305	0,0763
H₂O/HNO₃	0,267	0,267
H₂O	0,4002	0,4002
Total Weight	7,4304	7,2016

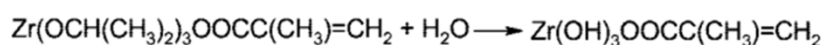
The following pictures (figure 10) describe the chemical synthesis of the Zr-hybrid. It is built in a sol-gel process as described in 2.2.1.



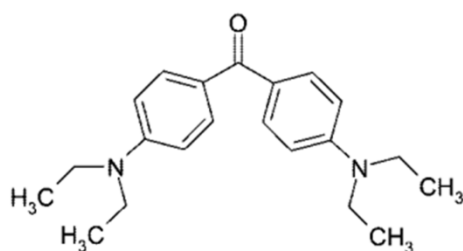
(a) MAPTMS hydrolysis



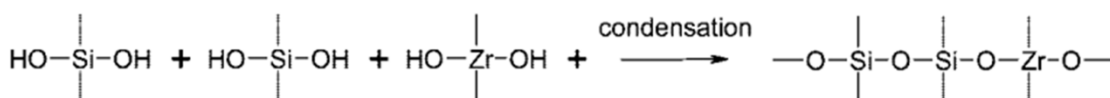
(b) MAA-ZPO complexation



(c) ZPO hydrolysis



(d) 4,4'-bis(diethylamino)benzophenone



(e) condensation

Figure 10 Chemical structures of the reagents leading to the formation of an inorganic matrix during the sol-gel process [15]

Before usage, the photoinitiator 4,4'-bis(diethylamino)benzophenone (BIS, fig. 10d) has to be added to all of the hybrid materials. For getting optimal basis material for structuring with 2PP, the solution has to be put in ultrasonic bath before preparation of the samples.

After preparing the samples by dropping the material onto glass substrates, the formulation has to dry properly. This drying process results in condensation of the 2-propanol and the formation of an inorganic matrix (fig. 10e).

Since previous experiments with this setup and hybrid materials were executed with 1% BIS [18], the experiments in this thesis also started with this concentration. However, as the project goal was to observe the interaction of the structures with cells, less PI concentrations were observed since this is assumed to be more

compatible. Possible residuals of PI not consumed during polymerization process can diffuse out of the structure and cause cytotoxic effects [20]. The PI-concentration in this context refers to percentage of Methacryloxypropyl trimethoxysilane (MAPTMS).

Tab. 2 Different PI-concentrations used for experiments in this work

Zirconium	1%	0,1%	0,05%	0,01%
Tantalum	1%	0,1%	0,05%	
Titanium	1%	0,1%	0,05%	

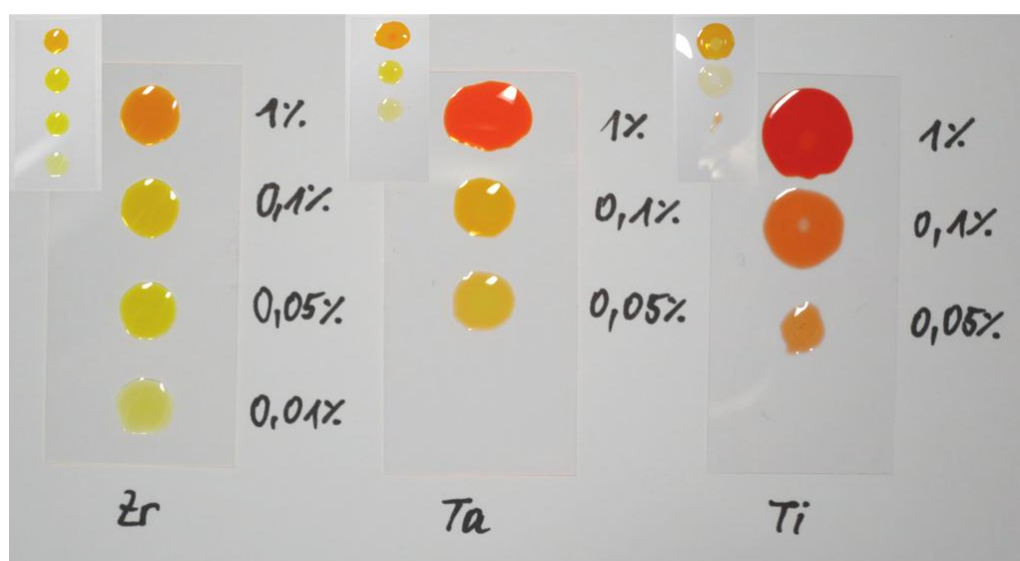


Figure 11 Colours of the hybrid materials with different PI-concentrations directly after application (small pictures) and after 4 hours of drying

Those materials are especially designed to have ultra-low shrinkage abilities [14, 15]. By adding MAPTMS (Methacryloxypropyltrimethoxysilane) and MAA-Zr (Methacrylic Acid) or ZPO (Zirkon n-Propoxid) to the sol-gels during the manufacturing process, a high stability of the hybrid photosensitive materials can be achieved.

4 METHODS OF FABRICATION OF MICRO- TO NANOSCALE PARTICLES

Structuring with 2PP allows to produce particles down to a size of 100nm [7]. However, this resolution is not only dependent on the hardware settings, such as stage system or objective. The whole appearance of the structures is in fact defined by settings like power, markspeed or hatching parameters.

Depending on the microscope objective used, the field of view (FOV) differs and therefore limits the writing area. Tabular 3 shows the dependence of the FOV on the optical system.

Tab. 3 Parameters of different objectives

	Zeiss 20x0.8	Zeiss 100x1.4
Magnification	20	100
Numerical aperture NA	0.8	1.4
Focal length FL [mm]	8	1.6
Back focal plane (BFP) diameter [mm]	12.8	4.5
Rectangular FOV [μm]	700	140
Circular FOV [μm]	500	100

$$FL = \frac{TL}{Mag} \quad (9)$$

$$BFP = \frac{2 \cdot TL \cdot NA}{Mag} \quad (10)$$

$$FOV = \frac{FN}{Mag} \cdot \frac{1}{\sqrt{2}} \quad (11)$$

Equation 11 leads to an available writing area of 100x100 μm for 100x1.4. Since the main goal in this thesis was to produce particles for cell studies, a high number has to be structured at the same time. This can be achieved by writing big arrays.

For fabrication of larger structures or when using files bigger than the writing field, the files have to be separated into smaller structures and then combined. This technique of combination of structures is called stitching [7].

To get as much structures as possible at the same time and use the available material to its full capacity, it is necessary to also extend the particle arrays in Z-direction. Unfortunately the resolution in Z is not as good as in XY-direction. The resolution in Z is defined by numerous parameters whereas the most limiting is the

free working distance of the objective which is defined by the distance between the front lens and the surface of the 150 μ m cover slip. Since we aim to also structure apart from the glass surface, the resolution in Z is also dependent on the numerical aperture (NA) which is a function of the refractive index (n) of the material between front lens and structure. To get as good resolution as possible, it is therefore advisable to use a material with an index of refraction similar to the cover slip. Consisting of glass, the coverslips used for these experiments have a refractive index of 1.52.

To make sure the available materials are suitable for vertical structuring, their refractive index (n) was measured.

Tab. 4 Refractive indices of the different hybrid materials

	liquid	(almost) dry
Zr-Hybrid (Sol A)	1,425	1,505
Ta-Hybrid (Sol D)	1,429	1,508
Ti-Hybrid (Sol F)	1,432	1,509

Since the measurement device (refractometer, Zeiss) is designed for liquid substances it is hard to measure n of the sol-gels. For getting as closest results as possible, the solutions are not completely dried. While controlling the change of n during the drying process, a raising tendency is observed. It is therefore assumed that the sol-gels have a refractive index of about 1.51 when dried. Although the Ti-hybrid Sol F seems to have the highest n compared to Zr and Ta, it will not get much higher since the Ti-sol-gels used in this experiments never dry completely, not even after a long time (one month) or when heated.

4.1 SAMPLE PREPARATION

The writing distance of the 100x/1.4 oil immersion objective requires using a high precision glass slide (150 μ m). Due to the objective's dimensions it is necessary to fix the cover slip below the object plate (metal plate in figure 12).

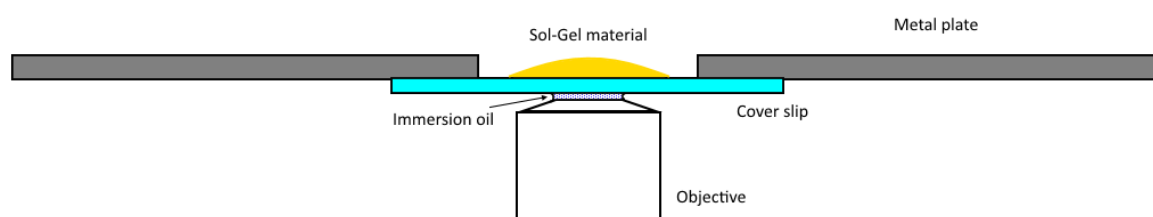


Figure 12 Scheme of the sample mounting

Depending on the intention – producing a high number of particles or just a few sticking to the glass – a 10mm or 18mm (in diameter) cover slip is used. Due to the

developing procedure it is preferable to either use a smaller slide (developing in Falcon® tube) or a bigger one (developing in petri dish). Also, if it is desired to get structures sticking to the glass, it is advantageous to first activate them with Trimethoxysilyl propyl methacrylate. For this activation (silanization) following steps are necessary:

- plasma clean (in slide rack) on “high” power for 3 minutes
- prepare silanization solution
 - stock solution: 48% EtOH (48ml), 0.3 % acetic acid (0.3ml), 50% water (50ml)
 - slowly add 2 mL **Trimethoxysilyl propyl methacrylate** dropwise
 - let stir for 30 minutes
- transfer slide rack with cover slips into stock solution
- let it in for 30 minutes
- wash with PBS
- let it dry

For the samples an amount of 20-30 µl of the material is dropped on the cover slip. It then needs a few hours to completely dry. This procedure can be accelerated by putting the glass slides on a heat plate at about 70°C. Same preparation procedure goes for petri dishes.

Due to the photoinitiator, the materials get colours in the range of yellow to red. The dryer it gets, the darker the colour becomes. Therefore it is easy to spot when the consistency is ready for use (see figure 11).

4.2 DEVELOPING PROCEDURE

To remove the non-structured part of the sol-gel, the sample has to be developed. For this procedure 1-propanol >99.9% (e.g. Sigma Aldrich 34871) serves as developing agent. This is then mixed with 2-propanol >99.9% (e.g. Sigma Aldrich 34965) to get a 1:1 dilution. The glass slide with the sample has then to be put in this dilution and left there for at least 30 minutes. It is most important to not let the sample dry in this stage since the undeveloped material causes the solution to be sticky which makes it difficult to work further. Therefore, the next step is to wash away the leftover monomers by carefully replacing the solution with new 2-propanol. To make sure the structures are clean, this step has to be repeated at least 4 times.

When producing structures for microscopy purposes they are usually little in numbers and sticking to the glass (here, mostly 18mm coverslip). Developing is best executed in a petri dish.

For developing a high number of particles, e.g. for experiments with cells, the procedure is changed. The developing dilution and the glass slide (in this case a 10mm coverslip) are put in a 15ml tube (Falcon®) for at least 30 minutes. Then the glass slide is removed and the particles spun down for 3 minutes at 1000 rpm. The particles are then visible at the bottom of the tube which allows removing of the propanol dilution as good as possible. Like before, the particles are washed a few times by filling the tube with 2-propanol and repeating the spinning. Since observing the interaction with cells is the main purpose of the particles, the propanol then has to be removed completely. This is achieved by applying vacuum till propanol is vaporized. The tube is then filled with *phosphate buffered saline* (PBS).

For further experiments with cells it is important to work sterile to avoid contamination.

After the developing procedure it is possible that the particles are still forming clusters. For better distribution, the tube is put in an ultrasonic bath (sonicator) for a few minutes. Ultrasonication should agitate and then disperse the particles evenly in the solution by applying sound energy.

4.3 STRUCTURING PARAMETERS

A .stl-file of the structures has to be uploaded to the software. It is then sliced into layers which then are fragmented into single lines. Hence, those lines define the movement of the stage/ laser beam and can be oriented in X- or Y-direction. After the .stl-file is loaded, various parameters have to be defined which are then crucial for the success of the structuring and quality of the results:

4.3.1 WRITING SPEED

Depending on which objective is used, the possible writing speed differs enormously (tabular 5). This is due to simple geometrical dependency. The scan angle speed is the same for all objectives. However, depending on the tube length the writing speed decreases, de higher the magnification gets. Tabular 5 shows the optimal and maximum writing speed for different focal lengths.

Tab. 5 Optimal and maximal writing speed for different objectives (focal lengths) [28]

f[mm]	250	160	8 (20x)	1.6 (100x)
Optimal	5.5 m/s	3.5 m/s	110 mm/s	35 mm/s
Fast	19 m/s	12 m/s	375 mm/s	75 mm/s

The optimal markspeed of the 100x1.4 objective would therefore be 35mm/s.

The software enables the variation of writing speed in an array.

4.3.2 POWER

The laser beam power has a large impact on the achievable structure size and resolution. Like written in 2.5 there are two polymerization thresholds for the power. Using the wrong power settings can cause either vanishing or destruction of the structures.

Those settings, however, have to be adapted for each material and their different compositions. Also, there is a dependence of the necessary power on the photoinitiator concentration [26].

The theoretical model for achievable voxel-size via 2PP can be described by its diameter [23]:

$$d = r_0 \left[\ln \left(\frac{\sigma_2 N_0^2 v \cdot \tau_L}{c} \right) \right]^{\frac{1}{2}} \quad (12)$$

with

$$N_0 = \frac{2}{\pi r_0^2 \tau_L} \cdot \frac{P \cdot \varphi}{v h \omega_L} \quad (13)$$

$$C = \frac{\rho_0}{\rho_0 - \rho_{thres}} \quad (14)$$

Symbol	Description
σ_2	cross-section of the 2PA
v	laser-pulse-repetition rate
τ_L	laser-pulse duration
r_0	focal diameter
φ	fraction of light transmitted
P	laser power
h	reduced Planck constant
ω_L	frequency of laser-light
ρ_0	wt. % of PI-concentration
ρ_{thres}	threshold concentration

Figure 13 Symbols used and their description

Consequently, the voxel-size and therefore the resolution of the structures is a function of various parameters, of which the laser power and the PI-concentration are the only parameters that can be easily tuned. Equation 12 allows to predict the behavior of the voxel-size for different PI-concentrations and power. It can be

shown that for lower power a smaller voxel can be achieved. For lower PI-concentrations higher power is necessary to get similar results.

4.3.3 HATCH AND DZ

To increase the stability of a structure, it is filled with a rectangular mesh consisting of lines. The so called “*hatch*” describes the distance between two of those written lines. This parameter highly depends on the achievable voxel-size, since for connected structures the single polymerized voxels have to overlap. A smaller voxel-size therefore requires a smaller hatch.

Further, the direction of hatching – the direction in which the single layers are divided – has to be determined. This can either be done in X- or Y- direction or in both. When hatching in X- and Y-direction the writing takes twice as long as when structuring in only one direction. The smallest available hatch is equal the resolution of the system and is about 0.1µm for this setup [7].

The number of layers which is used to divide the .stl-file depends on the dZ-parameter. It defines the distance between those layers. Like hatch, this specification depends on the voxel-size. However, the voxels are usually larger in Z-direction than in XY-direction which results in a lower axial resolution.

4.3.4 DELAYS

An RTC®5 PC-Interface card is used for positioning and processing of the galvo-scanner and laser. Since digital processing is executed quite faster than the movement of mechanical parts (inertia), delays have to be considered. If this is not done, writing-errors can occur during the 2PP-process. All delays wait till the movement of the mirror is finished before the next command is applied. Too short delays can lead to a transient response of the marked line (figure 14e) or the next command is applied before the mirror reaches its endpoint (figure 14f). Presuming too long delays, however, can lead to errors as well. If for example the LaserOff-Delay is too long, bubble formation can occur (figure 14d). Figure 14 shows errors which can occur when choosing the wrong delays.

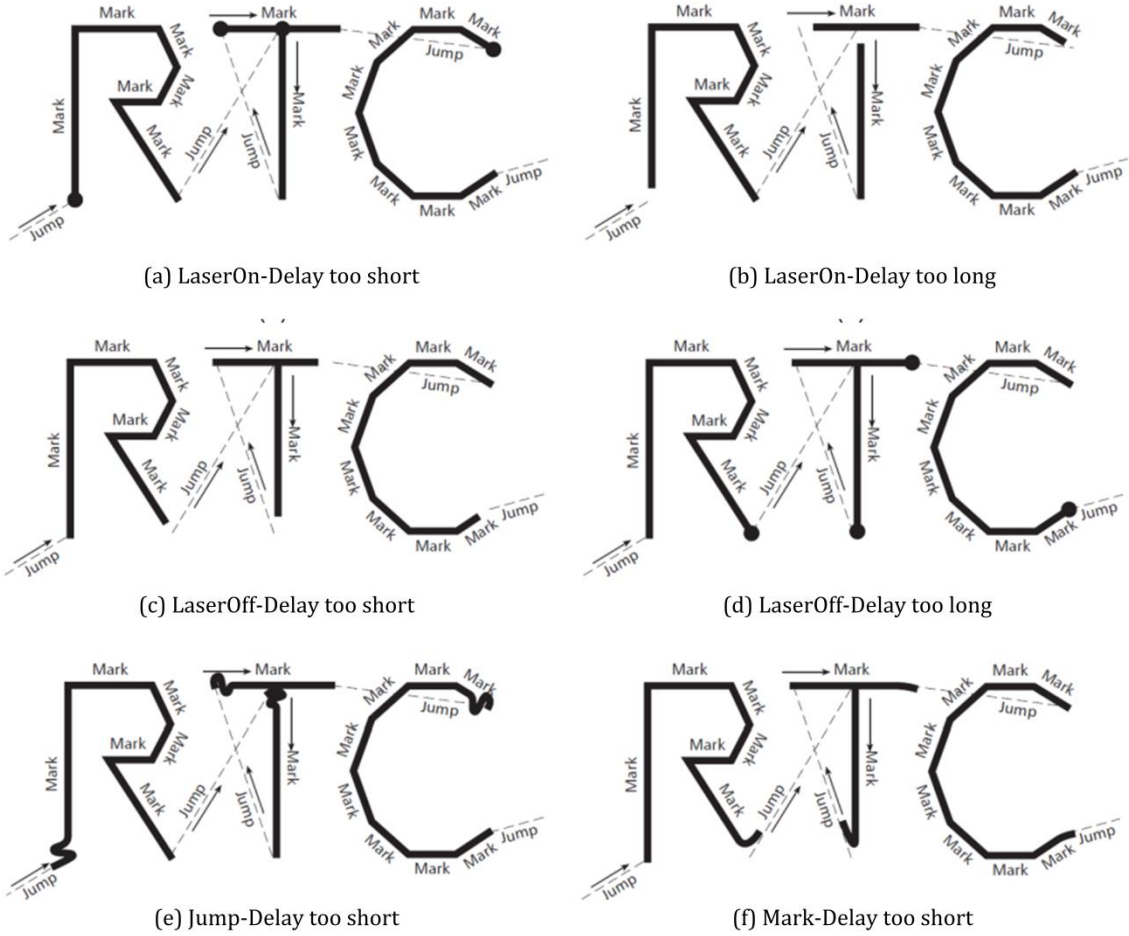


Figure 14 Different delays and their effects [24]

4.4 CELL COUNTING

Determination of cell concentration is required in various applications such as cell culture, microbiology, blood work and others. Since the actual amount of particles left after the developing procedure is unknown it would be helpful to count them or at least know the particle density in a specific volume.

When counting cells, a hemocytometer is often used. This counting chamber consists of a thick glass microscope slide which has a grid of perpendicular lines. The area covered by those lines is known, because of the specified dimensions of the grid. It is therefore possible to count how many cells there are.

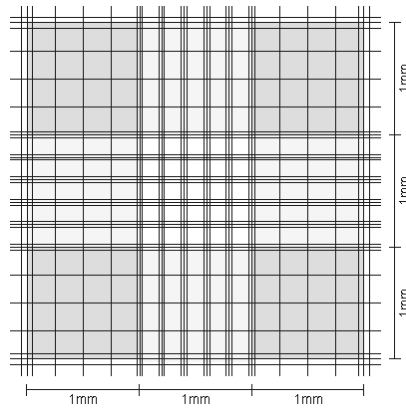


Figure 15 Neubauer-improved hemocytometer

When filling the hemocytometer, the coverslip has to be in place first. The sample is then expelled into the well and fills the area beneath the glass by capillary action. After a few minutes the counting chamber is then placed on the microscope. The full grid on a *Neubauer-improved* hemocytometer includes nine squares with 1mm^2 each (figure 15). Those squares are then further divided into subsection. The cells may then be counted.

4.5 CELL PREPARATION

For most experiments in this thesis, L929 cells of mouse cell line are used. The cells are fibroblasts and obtained from Sigma Aldrich. Those cells are well suited for cell culture. Other cells used are MC3T3, also of mouse cell line and fibroblast-like.

Dulbecco's Modified Eagle's Medium (DMEM) is used for all experiments. It contains high glucose (DMEM from Sigma Aldrich D1145) with 4500 mg/L glucose and sodium bicarbonate, without L-glutamine, sodium pyruvate, and phenol red, liquid, sterile-filtered, suitable for cell culture supplemented with 10% fetal bovine serum (Sigma Aldrich) and 1% of 10 000 U/mL Penicillin/Streptomycin (Lonza). The cells are cultivated in an incubator in humid atmosphere with 5% carbon dioxide at 37°C . The medium is usually refreshed every second day.

4.5.1 STAINING 1 – LIVE/DEAD STAIN

The LIVE/DEAD viability testing (Molecular Probes, Life technology) is used to assess cell viability according to manufacturer's instruction. The culture media is aspirated, the structures are rinsed 3 times in sterile PBS and then the staining solution with $0.2\ \mu\text{M}$ Calcein AM (live stain) and $0.6\ \mu\text{M}$ Propidium iodide (dead stain) is added for 20 minutes at 37°C . The samples are then washed with PBS and examined and photographed using laser scanning microscopy (LSM, Zeiss) with excitation/emission filter set at 488/530 nm to observe living cells (green) and 530/580 nm to detect dead (red) cells.

4.5.2 STAINING 2 – F-ACTIN STAIN

For better observation of the activities inside the cells other stains are used. Pre-staining the cells with Hoechst for the nuclei, later allows to determine if particles are on the same level or even inside the nucleus. This live staining has to be done before fixation since the cells are dead afterwards.

To investigate if the structures are entering the cells it is necessary to see where its borders are. For that the F-actin is stained which allows to see actin fibers. Fluorescent phallotoxins stain for F-actin (Life Technologies- A22287) is far red actin stain and can be examined using the LSM at 640nm.

The following protocol for F-actin staining was applied:

1. Wash cells twice with pre-warmed phosphate-buffered saline, pH 7.4 (PBS).
2. Fix the sample in 3.7% formaldehyde solution in PBS for 10 minutes at room temperature
3. Wash two or more times with PBS.
4. Cover cells with 1mL 0.1% Triton X-100 in PBS for 3 to 5 minutes.
5. Wash two or more times with PBS.
6. Add 200 μ L of 1% BSA, incubate 5-10 minutes
7. Dilute 1 μ L of fluorescent phalloidin (life technology A22287) in 500 μ L of 1% BSA
8. Incubate for 20 min
9. Wash 2 x with PBS
10. Image on LSM on Alexa 647 nm filter (red)
11. For further images store the plates with fix cells in the refrigerator in the dark

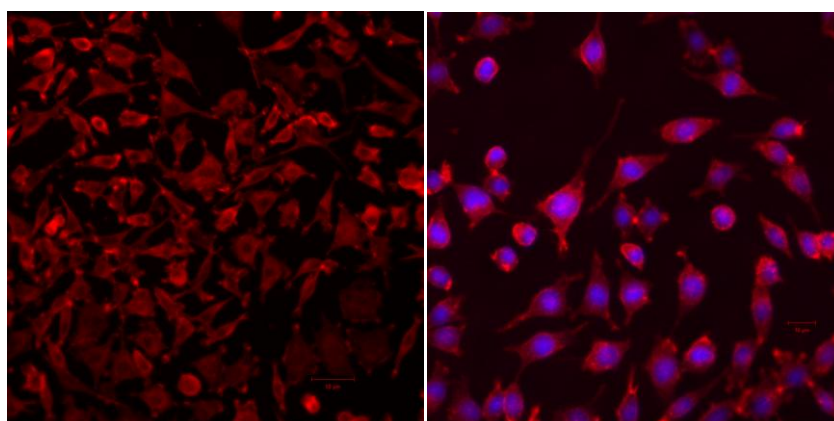


Figure 16 L929 mouse cells with F-actin stain (left) and F-actin + nucleus stain (right)

5 RESULTS AND DISCUSSION

Starting point of all experiments is a 3D-CAD-model of the particular structures. A .stl-file of this model is then imported into the software where all parameters are set. Except for the cell-experiments, which were prepared in glass bottom petri dishes, all samples were printed on high precision coverslips.

Former experiments with Zr-hybrid state that two-photon polymerization (2PP) provides a lateral resolution (XY-direction) of about 100nm and an axial resolution (Z-direction) of 1 μ m [7]. Those values can be confirmed and applied to other materials as Ta- and Ti-hybrids.

5.1 PREPARATION

Besides printing itself, the post-treatment of the structures is of high importance to get satisfying results. The very first step of the preparation is the developing process which can be the source of numerous issues. For the amount of material used for most of the experiments during this work (20-30 μ L) the developing time of 30 minutes was sufficient. However, for some samples this duration was not enough. Since the photoinitiator leads to a change of colour of the materials, it is easy to determine the stage of development. The coloured spot has to dissolve completely to ensure the removal of non-polymerized material. If leaving the samples in the developing solution for a too short period of time it is unavoidable that non-polymerized material is left. Those leftovers cannot be removed easily by flushing with 2-propanol afterwards, especially if the sample is dried somehow. Figure 17 shows a small amount of cubic particles of 1x1 μ m embedded in non-polymerized material. The particles though cannot be distinguished because of the leftover monomer which causes the whole sample to clump. Even putting the structures in 1-propanol for another 1 hour did not solve the problem. A too long developing time, however, leads to (partly) dissolving of the structures. This has an even bigger effect if the structures are written with low power or are very filigree. It is therefore recommended to not expose the structures to the developing solution for more than 4 hours. Also, storing of structures in propanol should be avoided. Figure 18 shows particles with stems left in 2-propanol for 2 days. The stems not only started to dissolve from the glass, but were also deformed. On the cubes, however, the propanol did not have great influence.

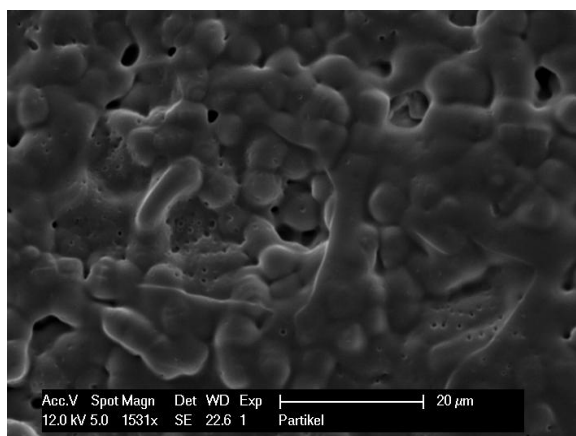


Figure 17 Sol A 1%; 1x1μm cubes; monomer not sufficiently washed out

Longer duration of developing may also cause other unpleasant side effects like vaporization of the solution. When the structures happen to dry completely during the developing procedure it is mostly unrecoverably damaged since the rest monomer causes the parts to stick together without a chance of disconnecting them.

To ensure optimal developing the sample should be moved from time to time (e.g. every 5 minutes). If the developing process is executed in a petri dish, which is done when producing structures sticking to the glass, a slight movement of the dish is usually sufficient. When producing a great amount of particles though, developing is done in a tube, which then has to be shaken in order to get all the particles off the cover slip. This procedure can lead to damaging or breaking of the coverslip in worst case or damage to the tube. As a consequence, parts of glass or polypropylene are floating in the solution, which have to be removed afterwards. It is therefore most important to ensure the removal of the coverslip before using the centrifuge. When spinning down the particles with the glass slide still in the tube the sample will most likely get unusable due to shattered glass.

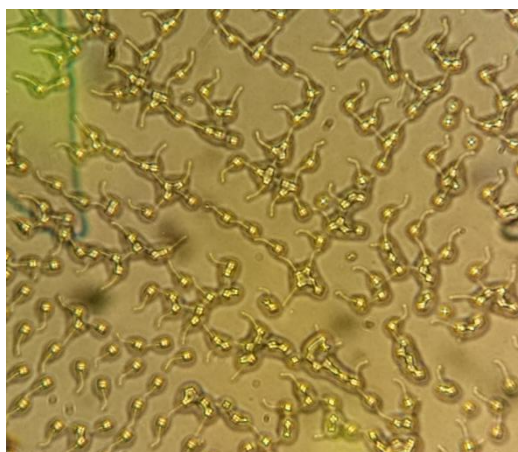


Figure 18 Sol A 1%; 5x5μm cubic particles with stems after 2 days in 2-propanol

Figure 19 shows what happens when structuring is done too close to the substrate. This especially happens when the glass slide is tilted or not mounted in a correct way. This phenomenon can occur when starting the structuring not deep enough inside the material and at the same time using the inverted dZ option. Although the particles in the solution usually do not suffer any damage, since the only deformed structures stick to the glass, a great loss of particles has to be accepted. In case of the sample on Figure 19 it was about a tenth of the whole amount of particles which was lost on the substrate.

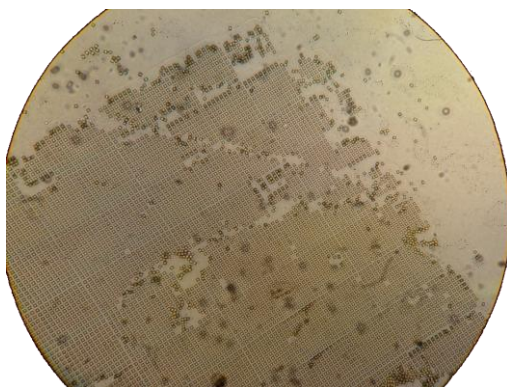


Figure 19 Sol A 1%; 5µm cubes on glass substrate. When structuring too close to the surface of the glass slide the particles tend to stick to the surface which then results in partly great losses

In order to remove dirt or other impurities resulting from the developing process the solution with particles can be filtered. Since the glass parts or dust particles are usually bigger than the structures, this should work theoretically. However, experiments showed that filtering only partly solves the problem, because big parts were filtered, but also a great amount of particles was lost in the net like shown in figure 20. To minimize the chance of dirt particles in the solution, the further experiments were then done with high caution. The coverslip was therefore rinsed with 2-propanol before being put in the sterile petri dish or tube. Developing was then done under sterile conditions.

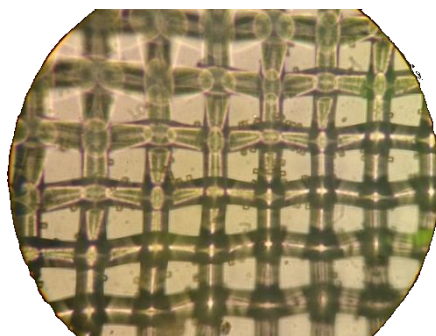


Figure 20 Sol A 1%; 5µm cubes in 40µm filter

After the actual developing step, the structures have then to be washed a few times with 2-propanol in order to completely wash out the rest monomer. Experiments

showed this should be done at least 4 times, depending on the purpose of the sample and the further experiments. When the next step is drying the sample for SEM examination it is sufficient to change the 2-propanol 3-4 times and then start exchanging it with HMDS.

More critical is the exchange of the propanol solution with PBS. When the non-polymerized material is not completely washed out, salts start to precipitate like shown in figure 21. Since the particles cannot be spun down when once in PBS and filtering is beyond question, those samples are then unusable for cell studies.

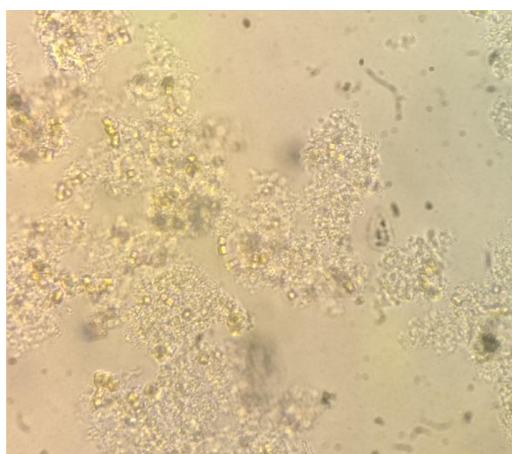


Figure 21 Sol A 1%; 5 μ m cubes in PBS. The remaining monomer was not washed out properly. This resulted in precipitation of salts when mixed with PBS

After the developing procedure it is most likely that particles are building clusters. To solve this, the tube can be put in an ultrasonic bath for 3-4 minutes which then dissolves the particle accumulation and leads to a better distribution in the solution. However, it is necessary to ensure that no residues of the glass slide are inside the tube since this would cause damage to the tube and to the structures.

Due to severe losses during the developing procedure itself, on the glass slide or during filtering it was tried to measure the actual amount of particles per mL. Although this was tried a few times, it was not possible to count the particles since they were not visible in the counting chamber. This can be either because they were too small to be found or never actually entered the chamber. Since particle loss occurred in previous steps already it is likely that the particles which were supposed to enter the counting chamber were lost in the pipette.

5.2 BUILDING SPEED

Although former experiments already provide results of speed tests [18] it was necessary to do further experiments concerning this matter. The aim of those tests was to find out for which speed the best results are achieved and if there are practical speed limits. Higher speed would result in shorter production time which would be favourable. Also, it was studied if there are any differences between the particular materials Zr, Ta and Ti concerning the outcome at certain writing speeds.

The tests were executed for all materials and the different compositions Sol A-G. Furthermore, the experiments were redone for a photoinitiator concentration of 1% and 0.1% BIS. The power was held constant at 40mW for the 1% PI-concentration and 60mW for 0.1%. Arrays of 10x10 cubes of 5 μ m side length and 5 μ m distance in between were printed slightly above the glass substrate. The height of the cubes was around 15 μ m.

The outcome for the different samples showed no big differences. Independent of material, the structures get clearer, the slower the writing is done. With higher markspeed the cubes become more round like shown in figure 22. This is due to a time delay at the beginning and end of the outer borders.

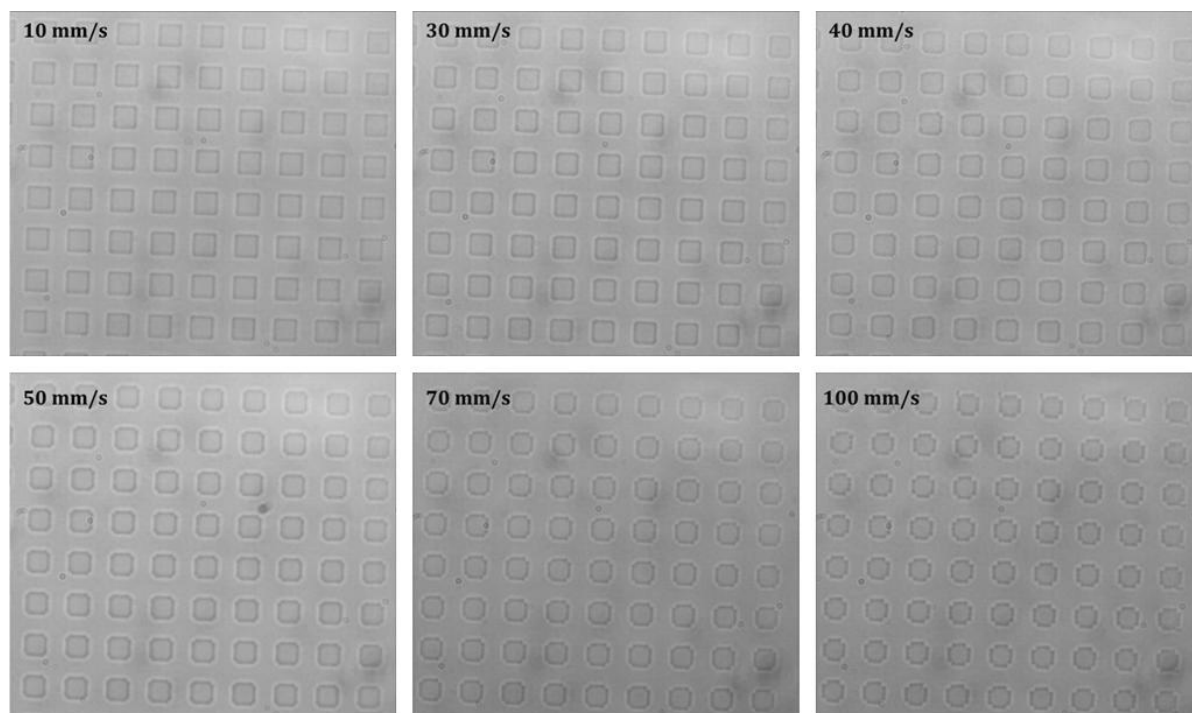


Figure 22 Sol D 0.1%; Arrays of 5x5 μ m cubes written with different speed at a power of 60mW each

The result of the former experiments done in [18] could therefore be confirmed. Choosing a writing speed of about 40mm/s proved to be a good compromise between accuracy of the structures and duration of the structuring. Higher

markspeed should be avoided if the shape of the fabrication is of importance. All following experiments were therefore executed at a markspeed of 40mm/s.

5.3 POWER

The laser beam power is one of the crucial factors for polymerization. One simple way to approach structuring would be to use a relatively high power - just below the point of destruction - to make sure the parts are fully printed. However, this is not constructive if the goal is to produce as small structures as possible.

Since the aim of the first experiments was to produce a high amount of particles and not especially small ones, the power settings were rather convenient. Figure 23 shows the LSM-image of some arrays of cubic particles, produced at 40mm/s and different power in Zr-hybrid with 1%BIS. The first complete array was obtained at a power of 50mW. For higher power (80mW and more) the cubes slightly got bigger and blurred.

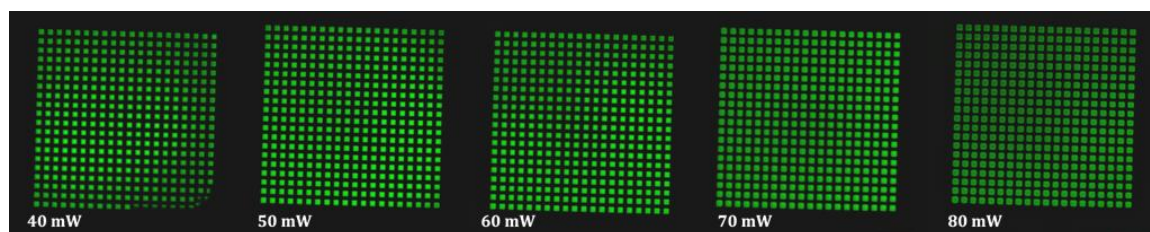


Figure 23 Sol A 1%; arrays of cubes written with 40mm/s; 40-80mW

The production of the particles was then done with 50mW for all materials at first. Zr- and Ta-hybrids seemed to be unproblematic when structuring big arrays (figure 24). Ti-hybrids, however, were more sensitive to power settings. Where 5mW were sufficient for Zr- and Ta-hybrids to localize the focal point on the camera image, Ti mostly needed at least 10mW to polymerize. It was therefore assumed, that higher power is necessary for Ti-hybrids to get satisfying results. Figure 25 shows the first experiments of printing the arrays with 60mW which resulted in burning and bubble formation though. The whole array was then deformed due to tension in the material.

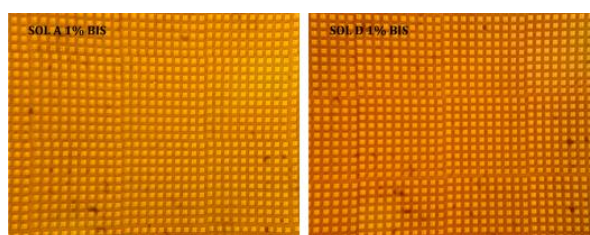


Figure 24 Sol A 1% (left) and Sol D 1% (right); Array of 5µm cubic particles, written with 50mW

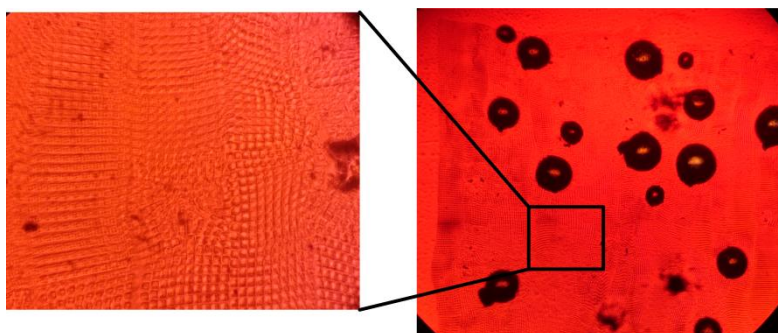


Figure 25 Sol G 1%; partly burned and deformed array of 5 μ m cubic particles, written with 60mW

In the beginning, all materials used had a PI-concentration of 1%. Structuring was done with 40-50mW for the samples with 1% BIS and adjusted if necessary, since the results can be immediately seen on the camera image.

As the main goal of the particle production is doing experiments with cells, the materials were diluted to get a lower PI-concentration in order to decrease the negative impact of the photoinitiator on the cells. First concerns, that a lower PI-concentration would result in problems for structuring could soon be eliminated. Although the required power for good results is higher, the lower the PI-concentration gets, structuring was successful. Tabular 6 shows the average power needed for getting satisfying results when printing arrays.

Tab. 6 Average power for good structuring results for different PI-concentration

	PI	[mW]	PI	[mW]	PI	[mW]	PI	[mW]
Zirconium	1%	40-50	0,1%	60	0,05%	60-70	0,01%	80
Tantalum	1%	40-50	0,1%	60	0,05%	60-70		
Titanium	1%	50	0,1%	60	0,05%	60-70		

Printing of smaller or single particles, however, resulted in different behaviour of the material concerning power. Some of those samples showed bubble formation and burning at lower power than before. It was therefore assumed that there is a correlation between power and time between the single layers. Theoretically, the smaller the structure or the faster it is written, the less time remains between the layers. Shorter intervals then should result in earlier burning since the material has less time to cool down in the meantime. Therefore, lower power should be used for higher markspeed. To study the relation between writing speed and laser beam power, the same test was done for all materials with a PI-concentration of 0.1%. Figure 26 shows a section of one of the first tests. Although the results seem to confirm the former assumption, they were not completely satisfying. Various problems occurred:

- *Reproducibility*: The experiments were repeated at least four times for each sample, but showed very different results every time.
- *Duration*: Although the parameters were constant for all samples, the total time of each experiment was different.
- *Burning*: Some bubbles were so immense that they destroyed a big part of the surrounding area. Structuring, where there is already a bubble, causes immediate explosion. This may explain, why burning sometimes happened at lower power than assumed.

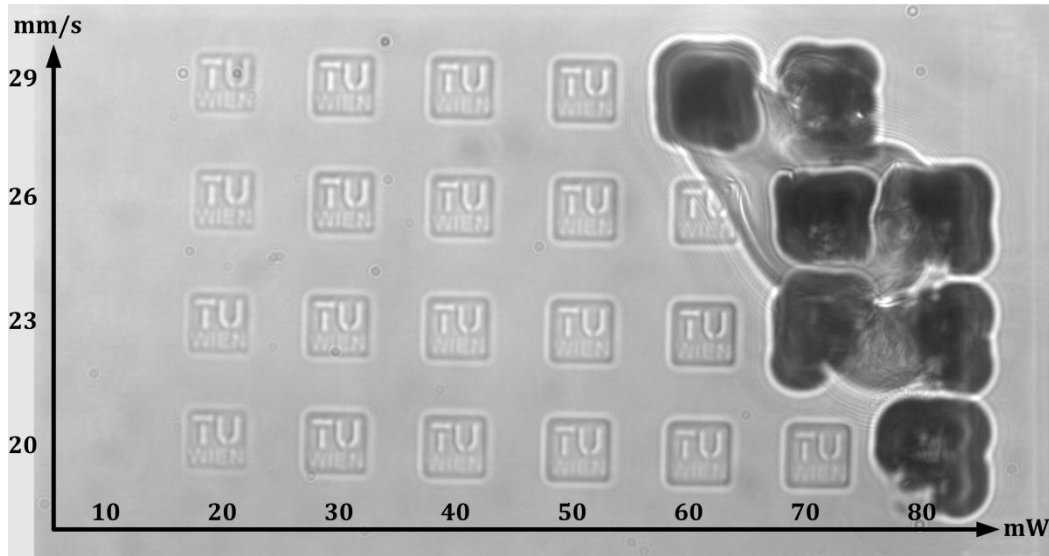


Figure 26 Sol A 0.1% TU-Logo of 10 μ m; 10-80mW, 20-29mm/s

Figure 27 displays the same experiment, but for two different structure sizes. In the left picture, the cubic structures had a side length of 10 μ m, on the right 5 μ m. Furthermore, a bigger distance between the single structures was provided to avoid accidental burning.

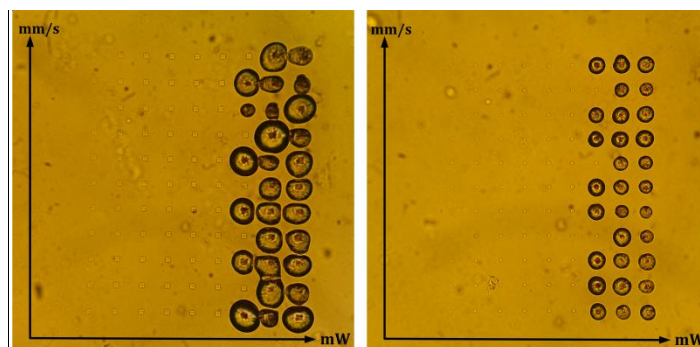


Figure 27 Sol A 0.1%; TU-Logo 10 μ m (left) and 5 μ m (right); Power 10-100mW and Speed 20—50mm/s (+10mW per column, +3mm/s per row)

Three repetitions were done for Zr, Ta and Ti each. Still, no significant results were obtained. Two main causes for that were then determined:

- *Software*: Due to computer operation, the laser randomly stops for a few seconds or parts of second. This then makes it impossible to define a relation between time and power, since the pauses are unpredictable.
- *Impurities*: Small air bubbles in the material or other impurities cause spontaneous destruction of the structures. This explains burning at low power.

The experiments were then repeated once more after a software update. The stopping could be eliminated. To avoid impurities in the samples, they were prepared in sterile environment. Figure 28 shows an array of 5 μ m cubic structures written with variable power and speed in Zr-hybrid material and a rating of the structures' quality. It was observed that for lower markspeed a lower power should be used. The higher the speed, the more the structures are deformed, like already observed in 5.2. However, higher power is required.

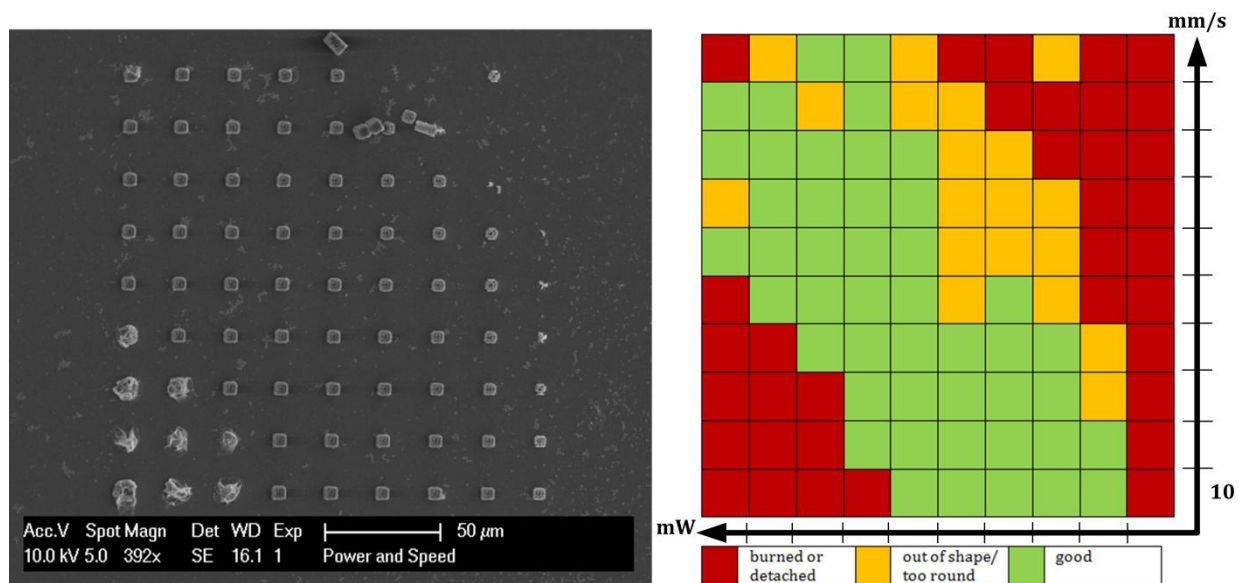


Figure 28 Sol A 0.1%; TU-Logo 5 μ m; Speed 10-100mm/s and power 10-100mW

The first assumption that lower power is needed for higher markspeed could not be proven. In contract, it is the other way round. Burning happened at lower power for lower writing speed. This is due to the laser beam being in the same spot for a longer time than when writing with higher speed. Too little power results in detaching or dissolving of the structures. The appearance of the array was quite similar for the different materials. For higher PI-concentration the maximum power was shifted to lower values.

5.4 POLYMERIZATION THRESHOLD

To measure the spatial resolution for the different materials with different photoinitiator concentrations a line test was executed. For this, blocks of 5x5 μ m

profile were built with thin lines between. Unfortunately, only the line tests with a PI-concentration of 1% showed expected results. In the other samples with a lower PI-concentration nearly all the lines were gone like shown in figure 29. Figure 30 and 31 show the results of the tests for Sol A, Sol D and Sol F.

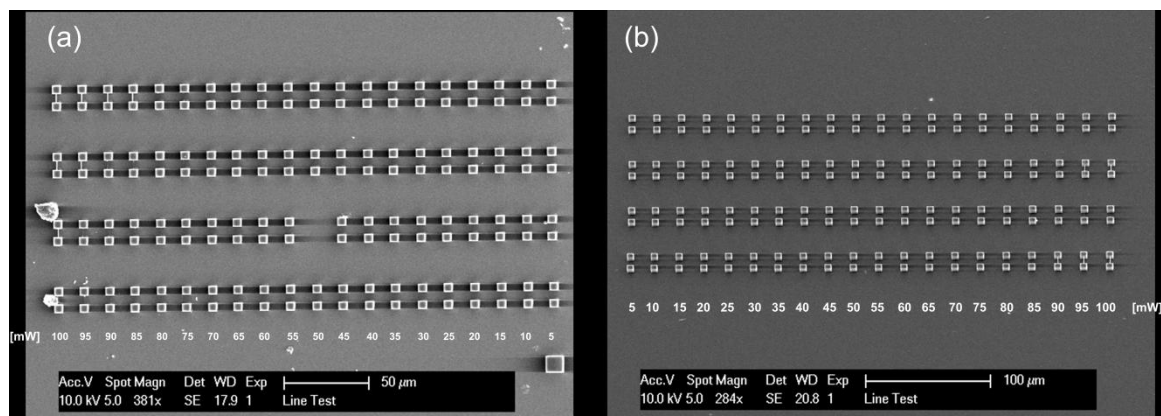


Figure 29 Line test for (s) Sol D 0.1%, (b) Sol D 0.05%

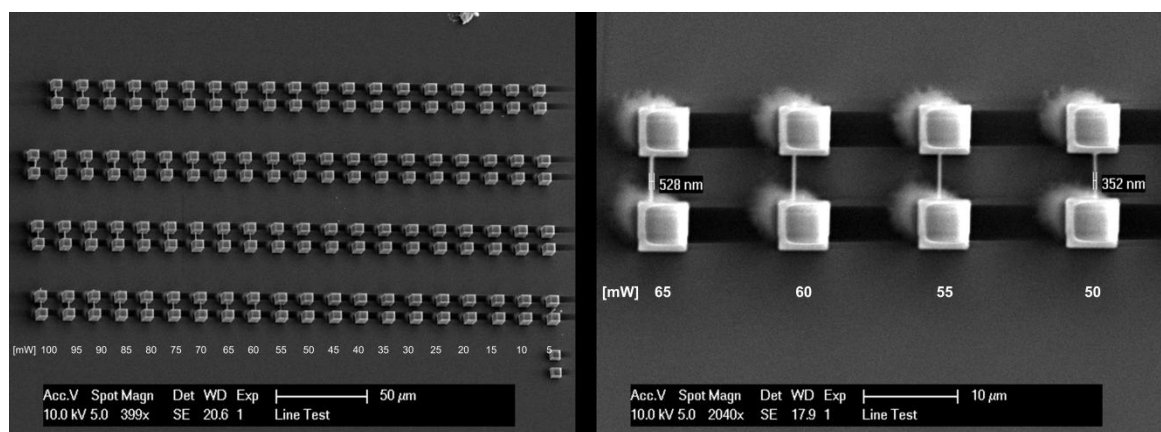


Figure 30 Sol D 1%; Line test

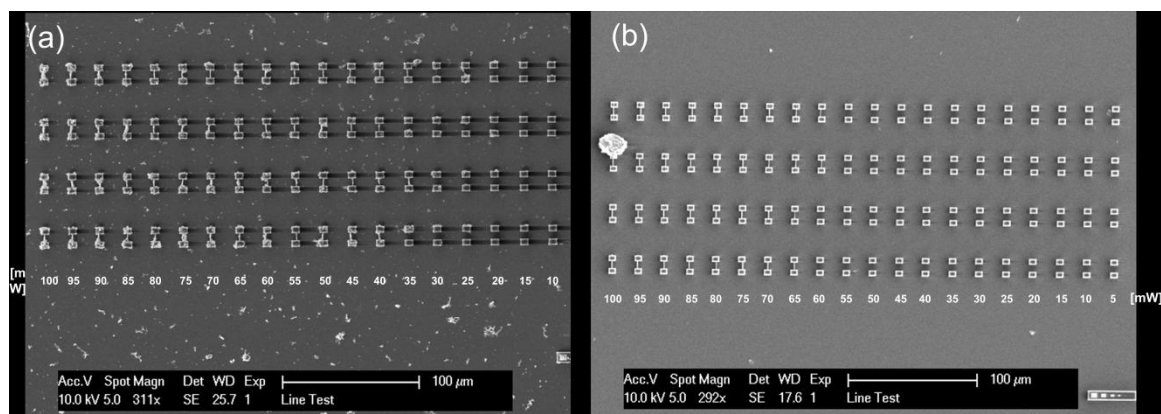


Figure 31 Line test for (a) Sol A 1% (b) Sol F 1%

5.5 LAYOUT AND HATCHING

When setting the parameters for the hatch, two decisions have to be made: the direction and the size. When constructing solid structures, hatching in either X- or Y-direction should be theoretically sufficient to ensure stability. This option, though, is only available in the newest software version. Lower size of the hatch should result in higher resolution of the structure. First experiments were done with a hatch of $0.3\mu\text{m}$ in X- and Y-direction. Figure 32 shows the first experiment of producing a non-cubic shape. The originally constructed pyramids have a base of $5 \times 5\mu\text{m}$ and a height of $4.3\mu\text{m}$. The produced particles, though, have a different appearance. Due to the axial resolution, they are higher than intended. Also probably due to the relative big hatch, clear steps are visible.

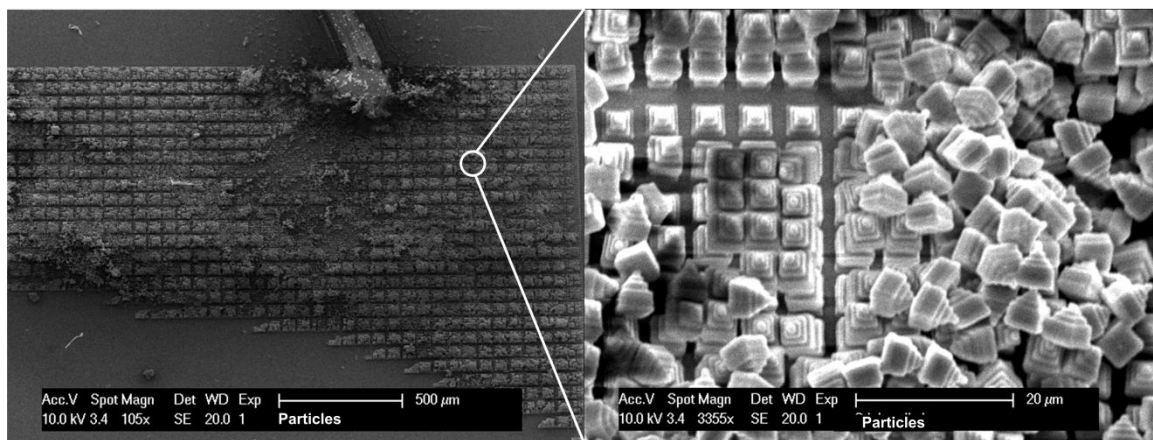


Figure 32 Sol A 1%; remainder of particles on a coverslip; pyramids with a $5 \times 5\mu\text{m}$ base

However, figure 33 displays a later experiment, executed after the software update. Here a hatch of $0.2\mu\text{m}$ and $0.1\mu\text{m}$ was set and done only in Y-direction. Furthermore, different markspeed – 20mm/s and 40mm/s – was used. There are six pyramids of different size printed on a foundation. Since there is no significant difference between the structures, the earlier observed steps may also be a result of internal software operations. Unfortunately, the resolution of the SEM is not high enough to get an image of the smallest pyramid on the sample. So far, no correlation of hatch size, direction, markspeed and resolution can be proven. Theoretically, though, the smallest structures can be achieved with the smallest hatch of $0.1\mu\text{m}$ at low power and markspeed.

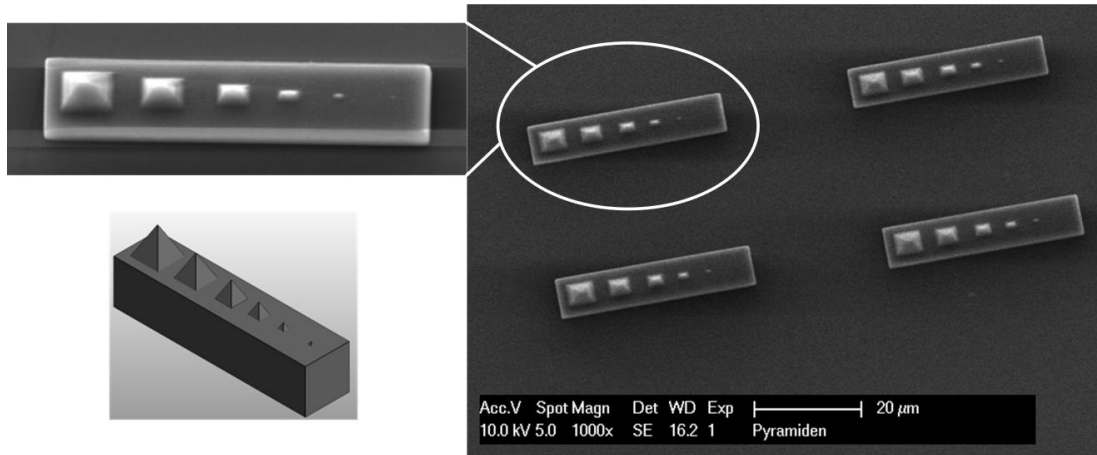


Figure 33 Sol A 0.05%; pyramids of different sizes on a foundation; size of the base from left to right: 5x5μm, 4x4μm, 3x3μm, 2x2μm, 1x1μm, 0.5x0.5μm

The direction of hatching becomes more important when writing thin lines. Figure 34 shows a part of the line test. Here the hatching was done in X- and Y-direction which resulted in crooked lines. Furthermore, hatching in only one direction is favourable because it only needs half the time for structuring compared to hatching in both directions.

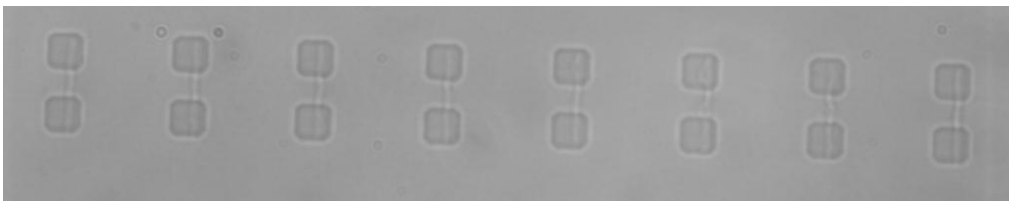


Figure 34 Sol D 1%; Free standing lines; 65-100mW; Hatch in X- and Y-direction

Printing of huge amounts of particles requires a consideration concerning file-layout. To get the maximum number of particles out of a sample, it is necessary to write three-dimensional arrays like shown in figure 36c. While the lateral size of the total array is limited only by the size of the sample, the height is limited by the depth of focus.

While the size of the lateral profile of the printed structures mostly corresponds with the actual size (size in .stl-file), the height of the particles often does not match. The STL-file of the cubic particles in figure 35a has a size of 5x5x5μm. While the lateral dimensions fit, the axial length is nearly twice as long as intended. The dZ-Parameter was set at 0.1μm which is the minimum value. However, the voxel-size in Z-direction is bigger than in X and Y which leads to a distorted structure. Therefore the axial resolution has to be concerned when designing structures.

Figure 35b shows the SEM-image of arrays of 1x1x1μm cubic particles. Those arrays consisted of 10x10x10 particles. The hatch was reduced to 0.1μm, which resulted in

a better width-to-length ratio. Still, the particles were out of shape. Here, this is due to a too small distance between the single particle-layers of the array.

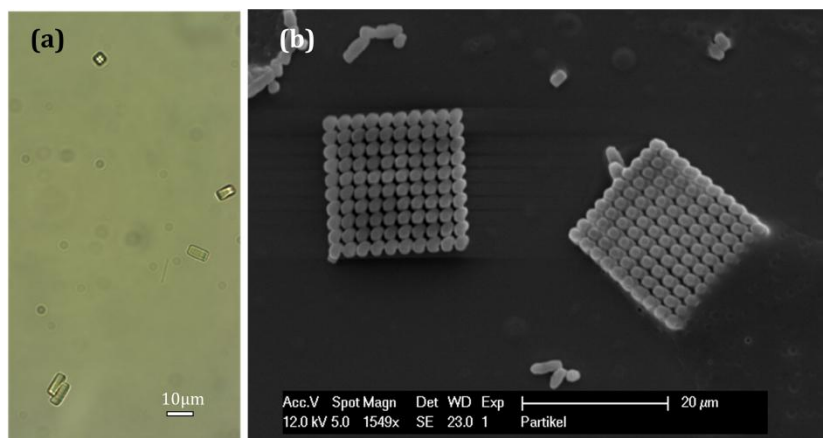


Figure 35 Sol A 1%; (a) 5x5μm cubes with a hatch of 0.3 μm and 0.1 dZ; magnification 63x, (b) SEM-image of arrays of 1x1x1μm cubes with a hatch of 0.1 μm and 0.1 dZ

If the distance between the layers of particles is big enough, but they are still sticking together after developing, it is possible to part them by putting the sample in an ultrasonic bath for a few minutes (figure 36 (a) and (b)).

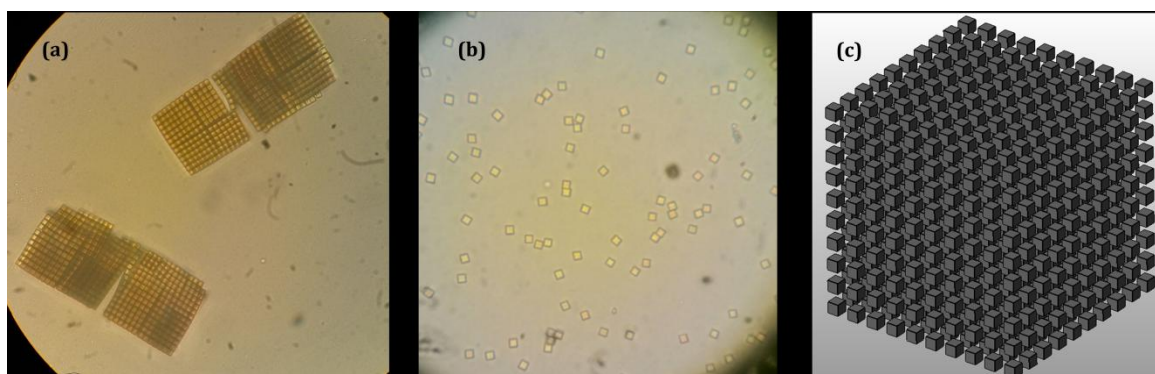


Figure 36 Sol D 1%; (a) arrays of 5μm cubes in 2-propanol after developing, magnification 20x (b) after sonification, magnification 40x (c) STL-file of cube-array

However, if the layers are too close, even sonication does not solve the problem. Figure 37 shows arrays of 1.25μm sized cubic particles after the developing procedure and after sonication. Sonication puts the single row apart, but due to too little distance in Z-direction the particles are melted together and stay in this form.

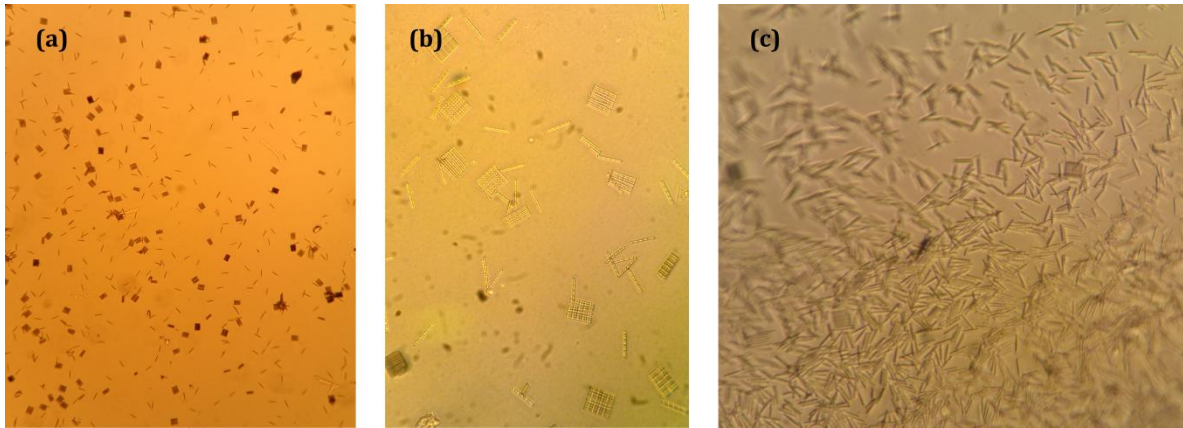


Figure 37 E 0.1%; (a) arrays of 1.25µm cubes in 2-propanol after developing; magnification 10x, (b) magnification 40x, (c) arrays of 1.25µm cubes after ultrasonication

Experiments showed that the distance between the particle-layer should exceed 1µm in order to avoid merging. In lateral layer, however, the particles could still be separated with a distance of 0.5µm. The requirement is a low power, since the structures tend to inflate with too high power (see 5.3).

5.5 FREESTANDING PARTICLES

For observing the interaction between particles and cells it should be possible to monitor the same cells over a defined period of time. To realize that, particles were fixed on a designated spot in a glass bottom petri dish. In order to avoid contact with the substrate the particles were given “stems”.

5.5.1 PARAMETER

The first experiments were done to evaluate the necessary parameters for the stems to stand and to stay fixed on the surface. They were executed for different power, particle size, distance between the particles and shapes of the stems. In figure 38, 5x5µm cubes on 50µm long posts with a diameter of 0.2µm are shown. To ensure that the particles have contact with the substrate, writing started a few micrometers in the glass, which is why the stems are shorter than intended. The printing was done at 30 to 100mW. However, right after developing all particles detached from the substrate, independent of power. Further experiments with different stem lengths and profiles were done, but showed the same results.

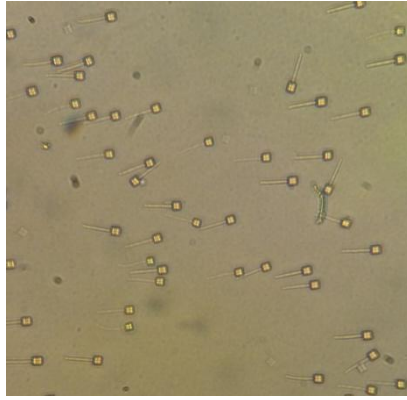


Figure 38 Sol E 0.1%; 50µm stems, 30-100mW

To avoid detaching, the glass – coverslip or petri dish – was functionalized (silanization with trimethoxysilyl propyl methacrylate, see 4.1). This immediately led to more satisfying results. However, although the particles were still fixed on the substrate, even after washing with 2-propanol, most had already fallen over. Like shown in figure 39 particles with longer stems tend to form clusters.

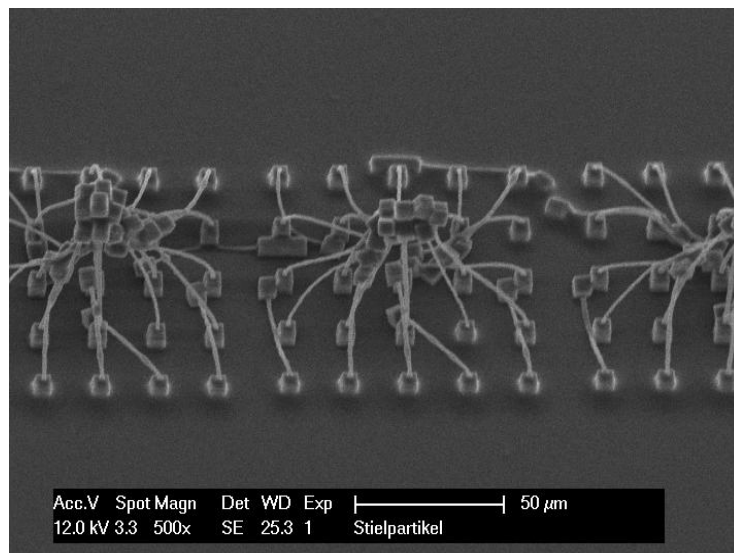


Figure 39 Sol C 0.1%; Cubic particles with 50µm long stems and small foundations to improve adhesion; the particles form clusters in the middle

The idea then was to construct posts with more stable profiles (figure 40c). In figure 40 an array of particles with different stem-parameters is shown. The same test was done for Ta- and Ti-hybrids and with different power settings. The appearance was similar for each sample. Stems with constant profiles were falling over (row 1-3 in figure 40a); the more massive ones seemed to be standing (row 4-6 in figure 40a).

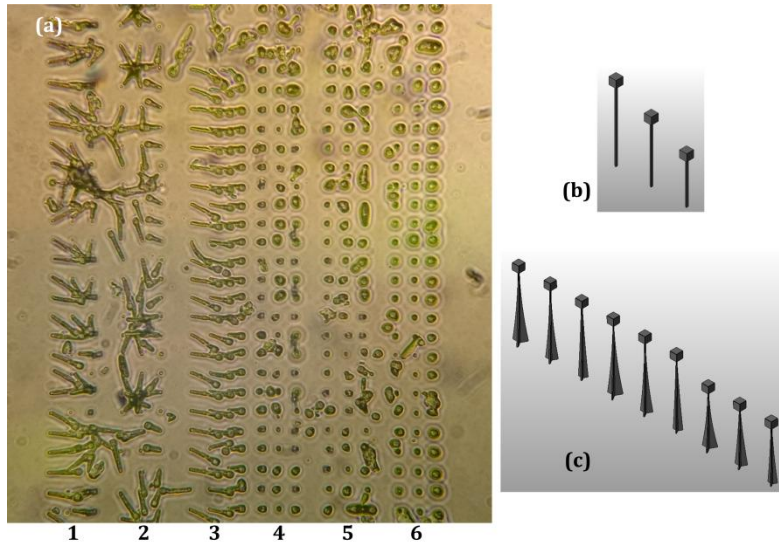


Figure 40 Sol A 0.1%; (a) Cubic particles on stems with different profiles, written at 90mW; stem-profiles from left to right: 1) \circ with diameter 1.5 μ m, stem length 50, 40, 30 μ m 2) \square with side length 1.5 μ m, stem length 50, 40, 30 μ m 3) Δ with side length 1.5 μ m, stem length 50, 40, 30 μ m 4, 5, 6) profiles like shown in (c), stem length 40, 50, 50 μ m, (b) stems with triangular profile and different length

The observation in SEM, however, showed different images. Even the more massive stems were completely or at least partially destroyed. Particles detached from the stems and ripped parts off. This phenomenon was observed, independent of material, power, size of the particles on top, and dimensions of the stems. Figure 41 and 42 show SEM-images of stem-particles, written with a power of 70-90mW, different profile dimensions and cube sizes of 3 μ m and 5 μ m.

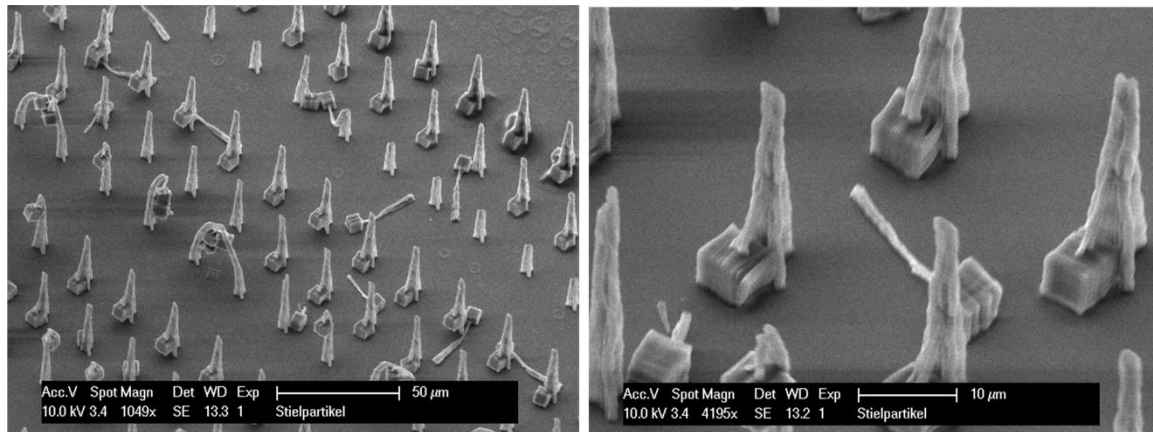


Figure 41 Sol A 0.1%; particles with different stem-parameters; 70-90mW (left) and 80mW (right) (0,7x30) with 5 μ m cubes

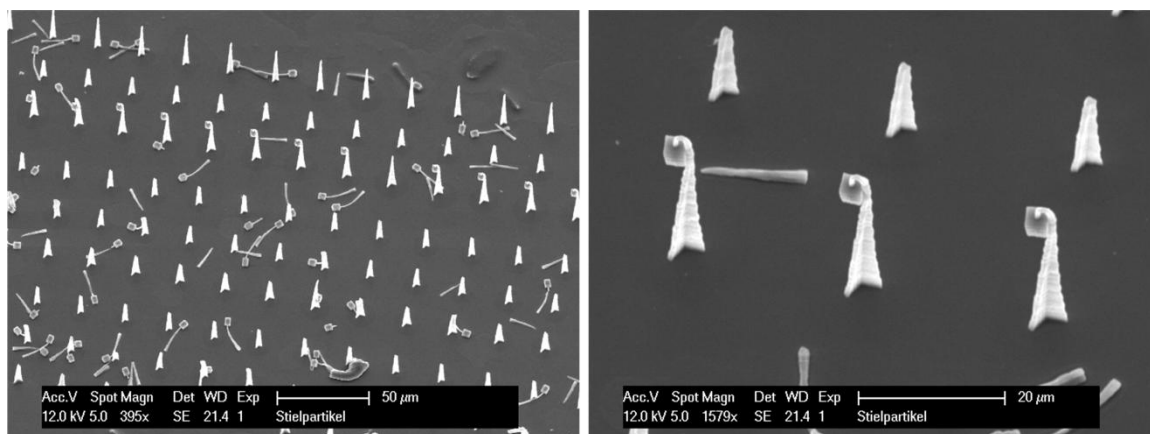


Figure 42 Sol A 0.1%; particles with different stem-parameters; 70-90mW (left) and 70mW (right) (0,5x50) with 3μm cubes

It was therefore assumed that the destruction of the particles is happening during the event of drying. The high surface tension when propanol vaporizes causes great damage. However, even when removing water the stems are damaged. During the developing and washing procedure, the particles are sometimes partly dried. Since the observation in the SEM requires drying of the sample, destruction was predestined. The further samples were then prepared with high caution to absolutely never dry the structures. The 2-propanol was then carefully replaced by PBS. In order to get images of the particles in PBS, the LSM was used. The experiments (figure 43) showed that all stem-particles, independent of the parameters, are standing. Even the particles with especially long and thin posts (figure 44) stayed upright.

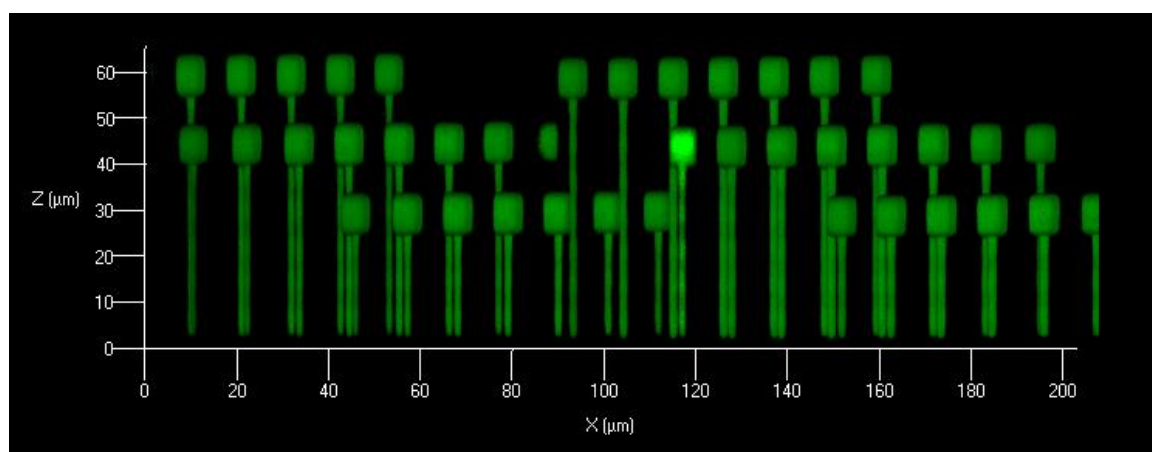


Figure 43 Sol A0.1%; particles with stems with quadratic (left) and round (right) profiles and a size of 1.5μm

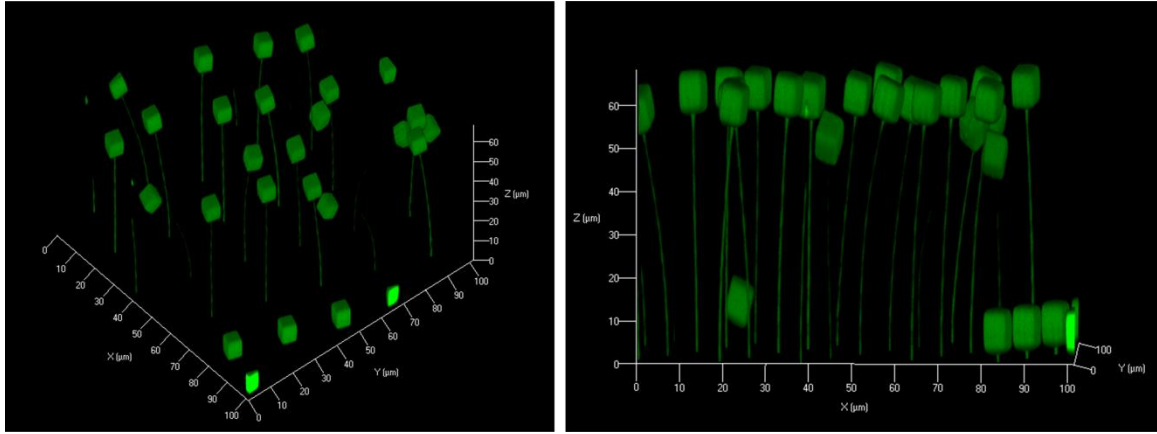


Figure 44 Sol A 0.1%; particles with 55μm long stems with a diameter of 0,2μm

The next experiments aimed to find out the necessary distance between the particles to not stick together. For this purpose, arrays of stem-particles were printed with various distances between the cubes. The biggest distance was 17μm, the smallest 5μm between the particles. Smaller distances resulted in errors in the software and were therefore skipped.

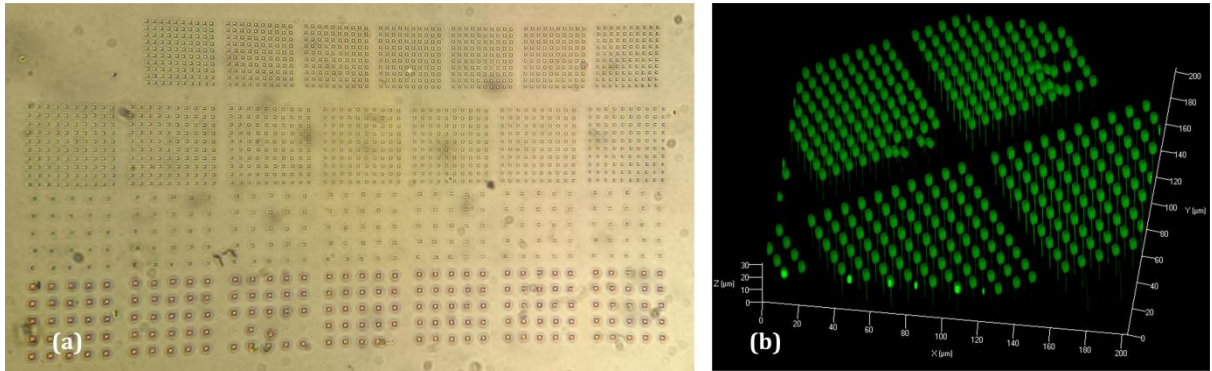


Figure 45 Sol A 0.1%; (a) from below: 5μm cubes with 17μm distance; 3μm cubes with 17μm, 7μm and 5μm distance between the cubes, (b) LSM image of the 3rd and 4th row (7 and 5μm distance), magnification 63x

The only sticking together was observed in the array with 3μm cubes and 5μm distance between them (figure 45b). However, it is assumed that even smaller distances are possible to achieve, as long as drying never happens.

5.5.2 LSM-IMAGES

In order to get high resolution and good images, the adjustments have to be done beforehand. For all LSM-images, a 63x/1.4 immersion oil microscope objective was used. Since the materials used are highly autofluorescent, the standard settings for laser beam are sufficient. Excitation was done at 488nm at 0.8-1%. The pinhole was set to about 40 nm and gain at around 600-700. Higher values should be avoided to not get overexposed images.

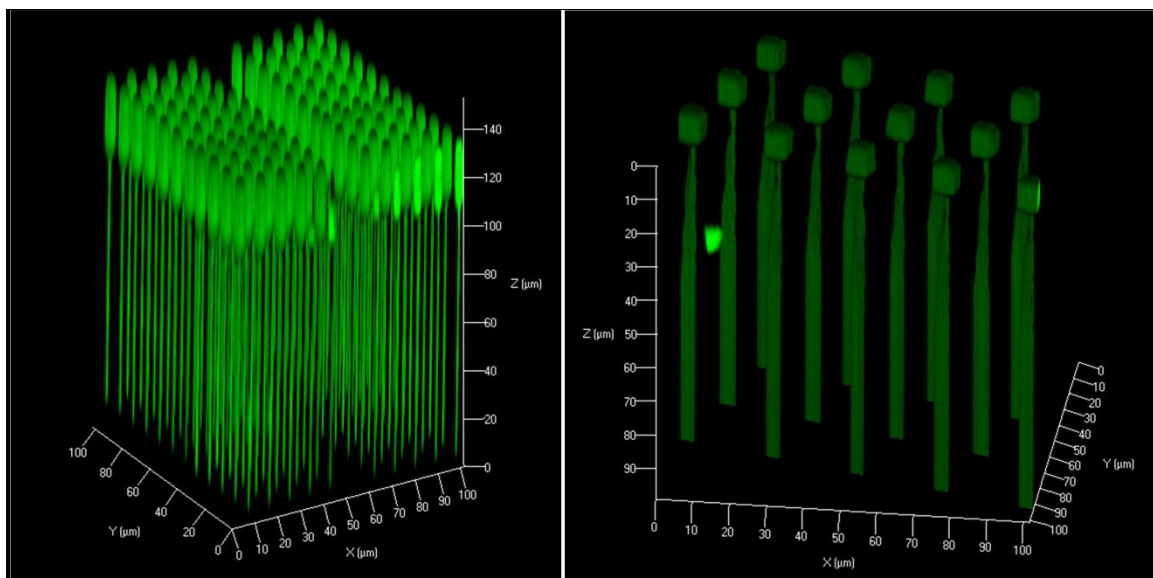


Figure 46 Sol B 0.1%; LSM picture of stem particles in PBS; due to wrong correction factor the assembly of the single layers is incorrect and the structures appear distorted; the actual length of the stems is 20μm, the particles are cubes of 3μm

Furthermore, the refractive indices of the materials should be considered. With a refractive index of 1.52, the immersion oil is synchronized for working with glass substrates. However, the refractive indices of air or PBS do not match with the immersion oil. Figure 46 shows the images of stem-particles in PBS without considering the different indices of refraction. The particles in the left picture should be at most 23μm high. The calculated high is 140μm though. This problem can be solved by calculating a correction factor r (see 4.3.1). The LSM-software then considers the different refractive indices when assembling the single layers. This, though, can still lead to unsatisfying results due to a low depth of focus when using media with highly different refractive indices.

To avoid distorted images, the 2-propanol or PBS can be replaced with thiodiethlyenglycol. With a refractive index of 1.52 it has the same as glass and the immersion oil. A much higher resolution in axial direction can therefore be achieved without concerning a correction factor which is 1 in this case.

5.5.3 STORAGE

Experiments should be preferentially done right after the developing procedure. However, clean working and careful replacement of the liquids can preserve the structures over a long period of time. While structures get distorted after only a few hours in 2-propanol (see figure 18), PBS causes little damage to the particles. Figure 47 shows stem-particles which were left in PBS over 50 days in a dark closet at room temperature. Although the shape changed a little – probably due to absorption of water – the stem were still fixed on the substrate and upright. Also the cubes were

still in shape. Thiodiethlyenglycol had a similar effect, but was only monitored for two weeks.

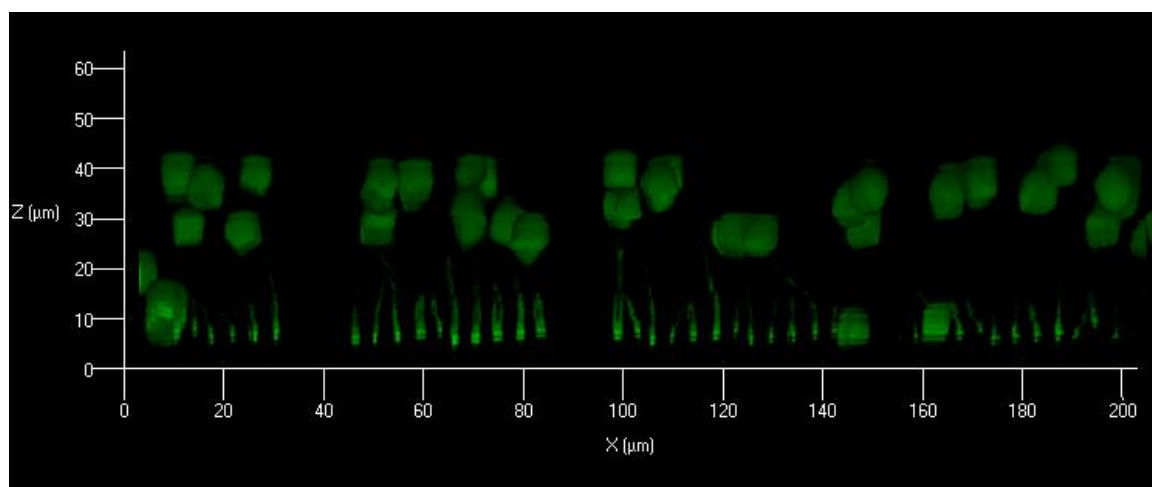


Figure 47 Sol A 0.1%; 5x5μm cubes on stems after 50 days in PBS

5.6 IN VITRO STUDIES

5.6.1 CYTOTOXICITY

To get an idea of the cytotoxicity of the materials used for structuring, the different substrates (Sol A, B, C, D, E, F, G) were put in a 96-well plate, dried and then exposed to UV-light for 20 minutes to initiate polymerization. The wells were then flushed 5 times with 2-propanol to remove the unpolymerized material. The substrates were then seeded with 10 000 L929 mouse cells per well. The viability of the cells was then compared to the cells seeded on the same 96-well plate without substrate.

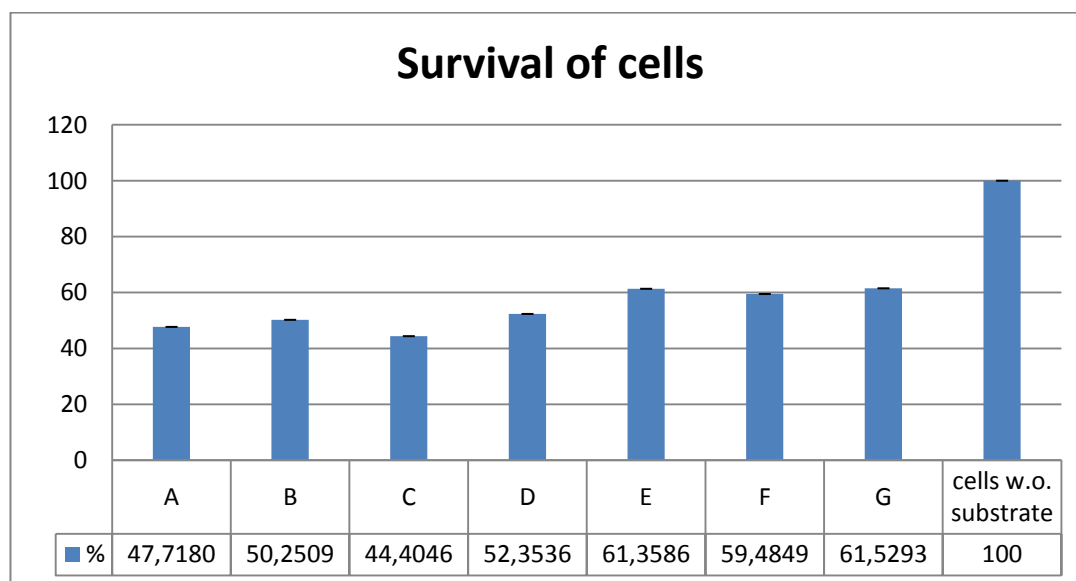


Figure 48 Survival of cells (L929, mouse cell line) on the different hybrid materials Sol A-G with 1%BIS

Figure 48 shows the results of viability testing of L929 mouse cells on the hybrid materials. The test was done for photoinitiator concentration of 1% which was the highest PI-concentration used for structuring. The experiment shows similar results for the different materials. It might be assumed that the Ti-hybrid (Sol F and Sol G) are less toxic and therefore more suitable for experiments with cells. However, this may be explained by the preparation of the samples for this test. Compared to the Zr- and Ta-material in the wells the amount of Ti-material was much less since a big part was washed away when flushing with 2-propanol. This can either be explained by a lower polymerization rate than Zr and Ta under the same circumstances or because the Ti-hybrid dried insufficient.

5.6.2 STAINING 1

Staining with calcein was the first try of getting images of cells interacting with particles. For those experiments, stem-particle arrays were printed in a functionalized glass bottom petri dish. The particles had 20 μm stems with 2x2 μm cubes on top. Developing was done as usual, but under sterile conditions. 2-propanol was replaced by PBS which was then exchanged 5 times to get rid of the 2-propanol completely. The particles were then seeded with 10 000 cells (L929 mouse cell line) each. After 4 days, staining was done.

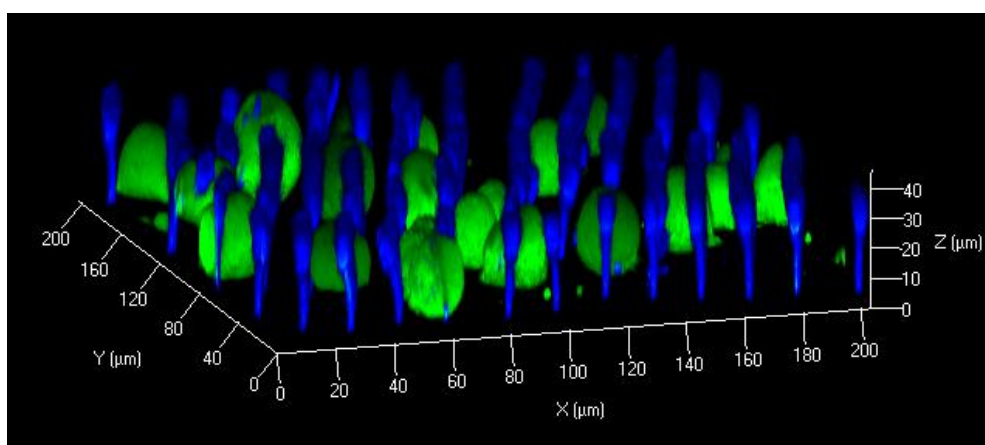


Figure 49 Sol E 0.1%; particles with stems seeded with cells (L929); Due to incorrect correction factor the indication of size is inaccurate

Due to the assumption that thidoethyenglycol would affect the cells, the examination was done in PBS. This resulted in inaccurate proportions of the 3D-images (figure 49). However, it can be observed, that the cells are not confluent, but rather round. Still, they seem to not avoid the particles. In fact, as can seen in figure 50, some bigger cells even tend to collect the structures.

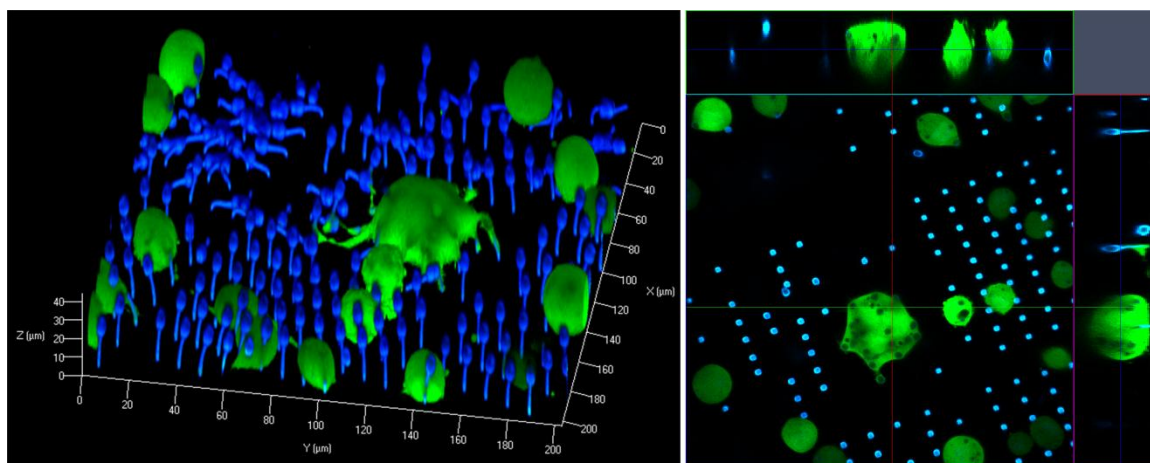


Figure 50 Sol E 0.1%; particles seeded with cells (L929); Bigger cells seem to collect the particles or at least grow around them

The biggest problem with this staining, though, was the autofluorescence of the particle-materials. The difference between excitation with a wavelength of 405nm (blue) and 488nm (green) is too small. The materials glow in whatever color they are excited which makes it difficult to distinguish between the structures and the cells (figure 51).

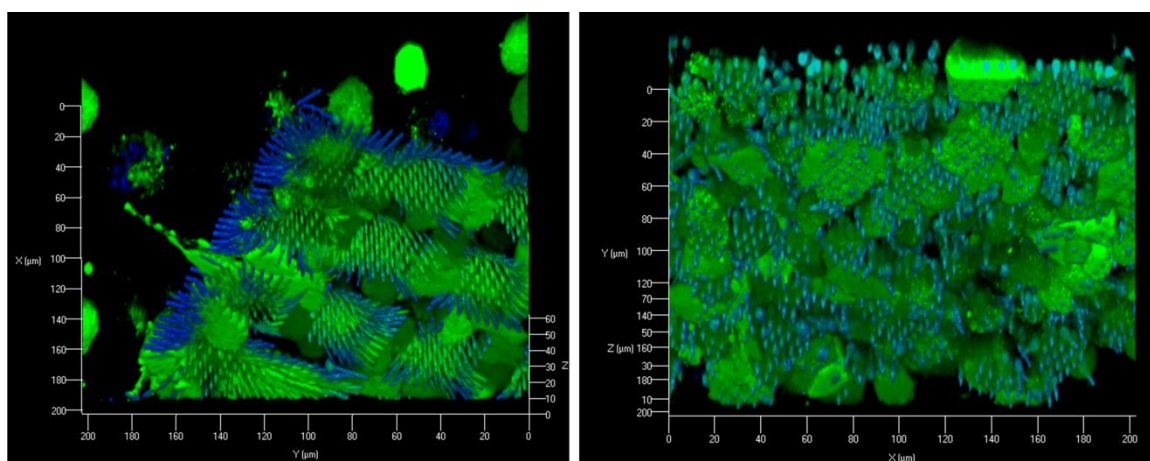


Figure 51 Particles seeded with L929; life stain; when too many cells are seeded on the sample it is difficult to distinguish between particles and cell since the hybrid materials are auto fluorescent and glow in whatever color they are excited

Tab. 7 LSM settings

	blue	green
Gain (Master)	892	648
Filters	BP 420-480	LP 490
Lasers	405nm at 0.89%	488nm at 1%
Pinhole	44μm	

5.6.3 STAINING 2

To get a better image of the interaction of the cells and particles, staining was now done for nucleus and actin. With this stain it should be possible to see if the particles are inside the cell. The particles were prepared like in the experiments before, with 20µm stems and 2x2µm cubes on top in a functionalized glass bottom petri dish. The samples were seeded with 10 000 cells each and left for 4 days. Medium was exchanged every two days. Since Hoechst staining for nucleus is life staining, this has to be done before fixing the cells. Afterwards actin can be stained. Excitation was done with 405 nm (blue, nucleus) and 639 nm (red, actin). For medium laser power the particles tend to glow blue.

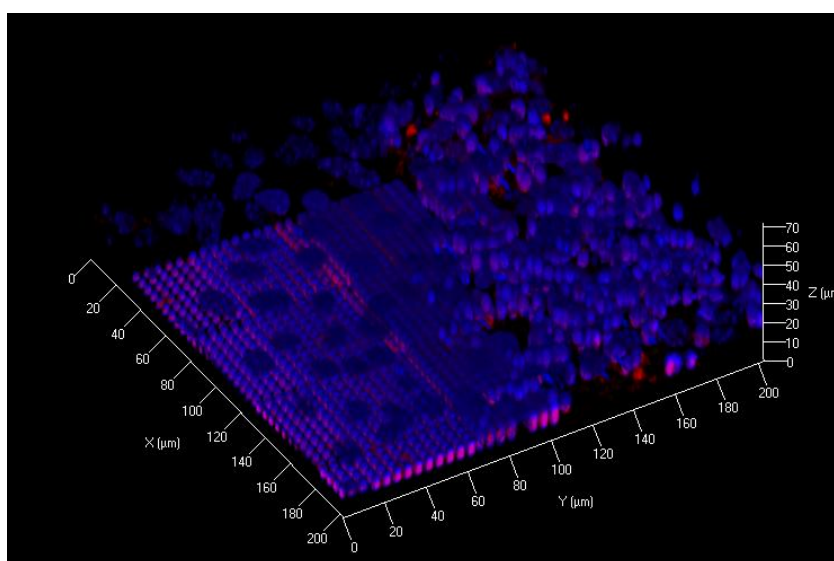


Figure 52 D 0.1%; Particles with stems seeded with L929 mouse cell line; Due to deficient actin staining the red parts are not visible despite maximum laser power at 640 nm

Tab. 8 LSM settings

	blue	red
Gain (Master)	775	855
Filters	BP 420-550	LP 640
Lasers	405nm at 1.8%	639nm at 85%
Pinhole	70µm	

The first experiments show that a more intense F-actin staining is necessary. Even at maximum power and reasonable pinhole size the red parts were not visible. Changing the master-gain to a higher value only caused artefacts. The red or pink parts visible in figure 52 are mainly artefacts or particles which start to glow red and blue for higher laser power. A more intense F-actin staining can normally be achieved by either using a higher dye concentration or longer incubation time. For the following experiments both was realized.

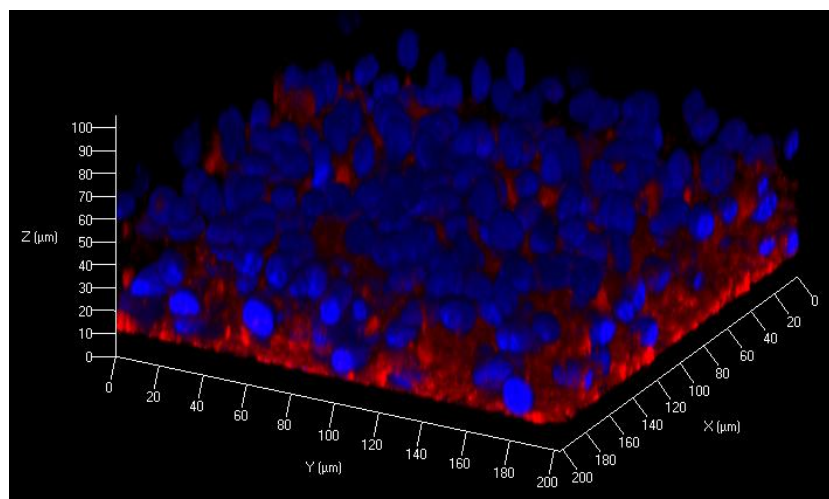


Figure 53 L929 mouse cells on a spot without particles; A too high number of cells makes it impossible to make a statement about particular cells

In figure 53 the red actin is visible. Still, the sample was not suitable for observations. Due to a very high number of cells, the particles could not be properly distinguished from the nuclei. Also it was not possible to make statements about particular parts of the sample or single cells.

Therefore samples with a low number of cells (4000 per petri dish) were prepared. Figure 54-57 show L929 cells from those samples. In the sample shown in figure 54, a big part of the particles were detached from the substrate and laying on the ground. Although the particles were not upright anymore as originally intended, the cells seemed to interact with the structures. Single cells were collecting the particles including their stems.

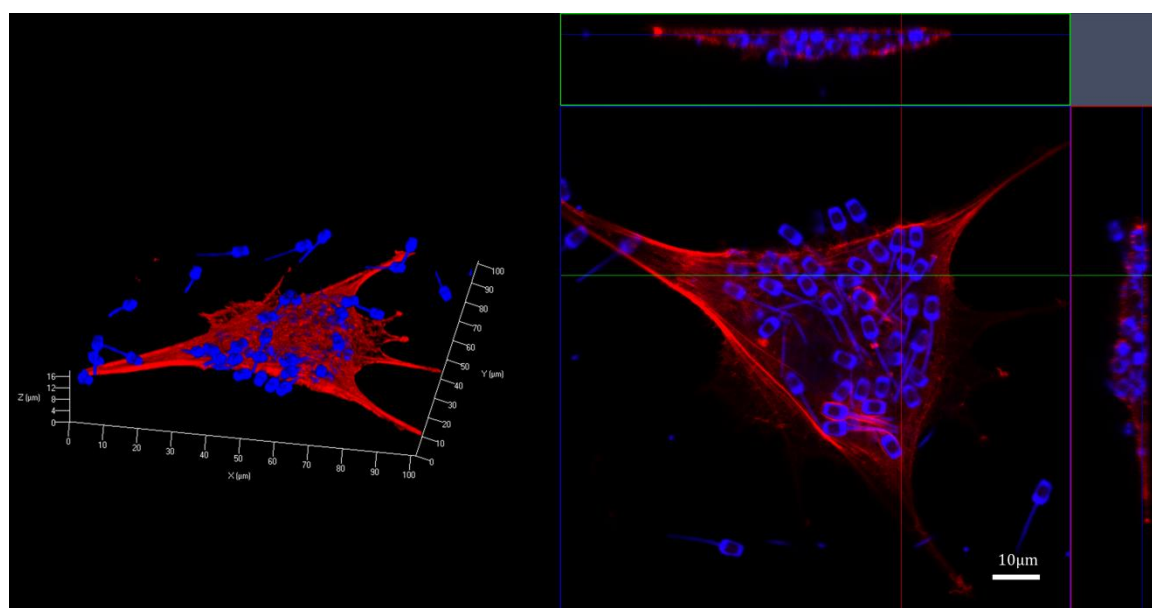


Figure 54 Sol E 0.1%; 2x2μm cubes on stems seeded with L929 mouse cells; stained for F-actin and nucleus; Right image: sectional view of the cell

Tab. 9 LSM settings

	blue	red
Gain (Master)	551	630
Filters	BP 420-550	LP 640
Lasers	405nm at 0.8%	639nm at 7%
Pinhole	47 μ m	

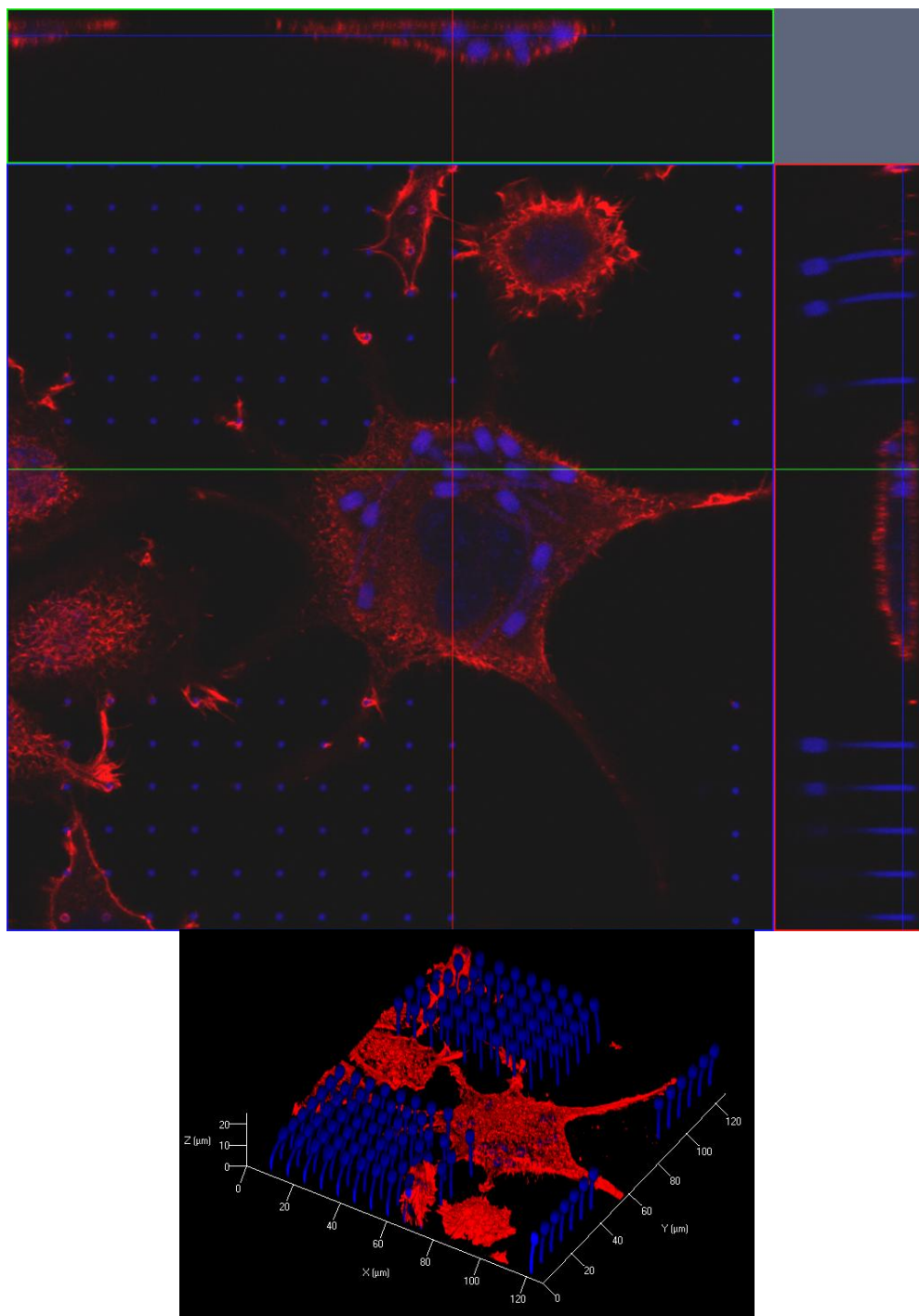


Figure 55 Sol B 0.1%; 2x2 μ m particles on 20 μ m stems (blue) fixed on a glass-bottom petri dish and seeded with cells (L929, red); Staining: Actin (red) and nucleus (blue)

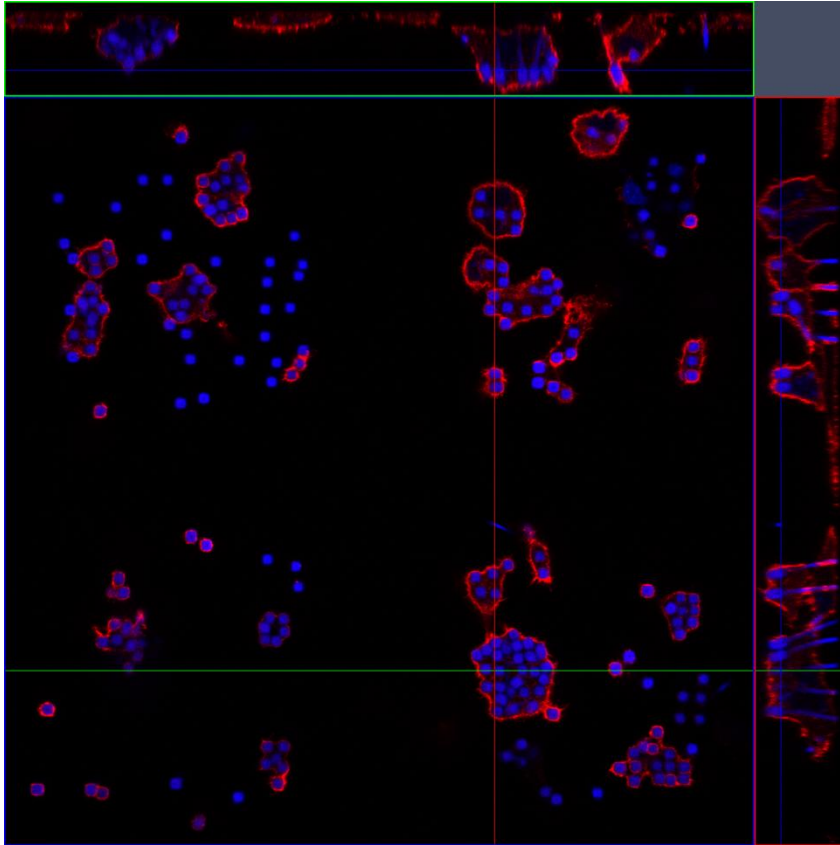


Figure 56 Sol B 0.1%; 2x2 μ m particles on 20 μ m stems (blue) fixed on a glass-bottom petri dish and seeded with cells (L929, red); Staining: Actin (red) and nucleus (blue)

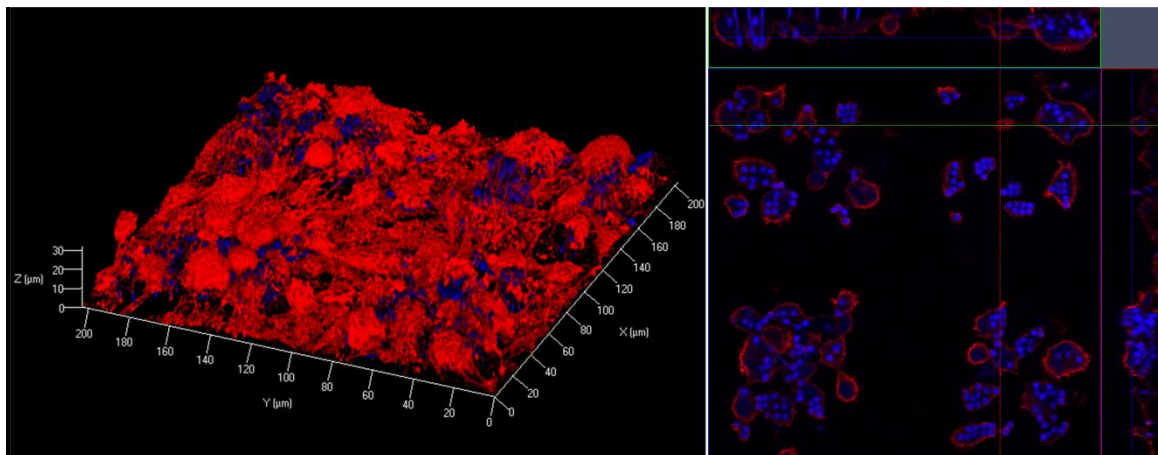


Figure 57 Sol B 0.1%; 2x2 μ m particles on 20 μ m stems (blue) fixed on a glass-bottom petri dish and seeded with cells (L929, red); Staining: Actin (red) and nucleus (blue)

For a final experiment another four samples were prepared. The goal of this experiment was again to find out if and how the cells are interacting with particles. since the former experiments where all executed with the same cell line (L929) it was of great interest if there is a different reaction with other cell types. In order to find this out MC3T3 mouse cells were used. For observation purposes the particles were again located on top of posts while those were fixed on the glass. Also, to find out if there is a different behaviour when cells get in contact with only the posts

without particles on top, a few arrays with post-only structures were printed. Last but not least another two samples were prepared with only particles.

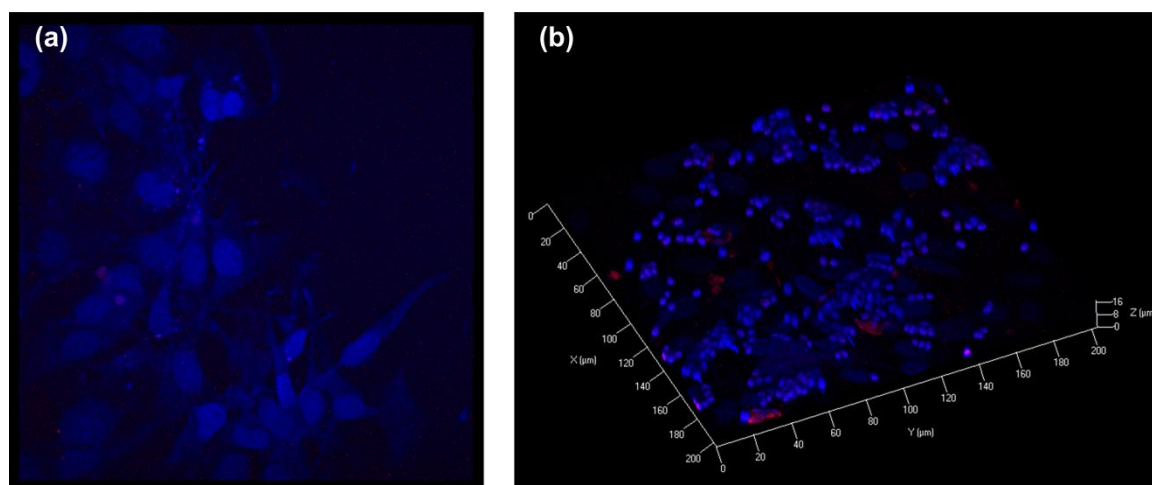


Figure 58 (a) MC3T3 cells with 1µm cubic particles (Sol B 0.1%), (b) Sol A 0.1% particles with stems, seeded with MC3T3 cells; actin stain is not intense enough to be visible

The examination on the LSM, however, showed not the expected results. In the samples with only the particles and cells, no particles could be found (figure 58a). The other samples with stems and stems with particles on top, also looked quite different than before. This may be again caused by insufficient F-actin staining. Therefore no predication can be made concerning the cell interaction with only particles or stems.

6 CONCLUSION

It was shown that particles with a size of below $0.5\mu\text{m}$ can be fabricated, using an appropriate two-photon polymerization setup. The size of the volumetric pixels has the biggest influence on the particle's dimensions and resolution. It is highly dependent on the laser beam power and photoinitiator concentration. Because of the elliptic shape of a voxel, the resolution in lateral directions (X and Y) is higher than in Z-direction. The smallest voxel-size, however, could not be determined with the experiments during this thesis, due to insufficient resolution of the microscopes used. Also, the fabrication and drying process has to be improved for further experiments in order to ensure the preservation of the lines. Still, even for very low PI-concentration of 0.01% BIS, it could be shown that structuring is possible. Lines with a thickness of about $0.1\mu\text{m}$ can be achieved.

The easiest way to get a better resolution is using a microscopy objective with a higher numerical aperture. Nowadays, immersion oil objectives with NAs of up to 1.65 are available. With those, a significantly higher resolution in axial direction can be achieved.

To get structures of a defined form, it is advisable to make them at least $0.5\mu\text{m}$ big. This is enough to fabricate simple geometries such as blocks, pyramids or spheres. For more complex structures, a size of at least $1\mu\text{m}$ should be contemplated. Smaller structures can be produced, but do not – as far as we know – have the desired shape. Furthermore, the design of the parts has to be adjusted in axial direction, since especially on such small structures, the axial resolution has a great influence. For this particle size, hatching in only one direction – either X or Y – is fully sufficient, since the smallest hatch of $0.1\mu\text{m}$ or at most $0.2\mu\text{m}$ is used and it is assumed that the smallest voxel-size is slightly bigger. Hatching in both directions neither raises the stability of the structures nor has a great influence on the appearance. In fact, it only doubles the writing time.

As for writing speed, it can be shown that 40mm/s is a good compromise between duration of the fabrication and accuracy of the structures. Even big amounts of structures can be written in a reasonable period of time. Printing of $5\times 5\mu\text{m}$ cubes for example took 15 hours for around 3 million particles. With improvements of the software processing – especially regarding delay-management – it may be possible to even print with higher speed.

The experiments with cells showed that there is a tendency of the cells to collect the particles. Whether the structures are sticking out of the cell membrane, the cells grow around them, or the particles really are inside of the cells cannot be told at the time. To make explicit statements, far more experiments have to be done. More

different structure geometries, sizes and PI-concentrations have to be tested. Furthermore, the behaviour of other cell lines should be observed. However, it could be shown, that the materials used were not toxic and caused not harm to the cells. In fact, the cells seemed to have an affinity to the particles. An effective influence on their activity and properties has yet to be shown.

7 BIBLIOGRAPHY

- [1] R. J. Young, P. A. Lovell: *Introduction to Polymers*. 2nd Printing of 2nd Ed., CRC Press, 2000.
- [2] Passinger, S.: *Two-Photon Polymerization and application to Surface Plasmon Polaritons*. Hannover: Cuviller Verlag Göttingen, 2008.
- [3] Sperling, L.: *Introduction to Physical Polymer Science*. 4th ed. Wiley-Interscience, January 2006.
- [4] Melchels, F.P., Feijen, J. and Grijpma, D.W.: *A review on stereolithography and its applications in biomedical engineering*. Biomaterials, vol. 31, no. 24, pp. 6121 – 6130, 2010. ISSN 0142-9612.
- [5] Göppert-Mayer, M.: *Über Elementarakte mit zwei Quantensprüngen*. Annalen der Physik, vol. 401, no. 3, pp. 273–294, 1931. ISSN 1521-3889.
- [6] Kaiser, W. and Garrett, C.G.B.: *Two-Photon Excitation in $\text{CaF}_2:\text{Eu}^{2+}$* . Phys. Rev. Lett., vol. 7, pp. 229–231, Sep 1961.
- [7] Gruber, P.: *High speed fabrication of large scale membranes by means of two-photon polymerization*, Master thesis, TU Wien, 2013
- [8] Haske, W., Chen, V.W., Hales, J.M., Dong, W., Barlow, S., Marder, S.R. and Perry, J.W.: *65 nm feature sizes using visible wavelength 3-D multiphoton lithography*. Opt. Express, vol. 15, no. 6, pp. 3426–3436, Mar 2007.
- [9] Juodkazis, S., Mizeikis, V., Seet, K.K., Miwa, M. and Misawa, H.: *Two-photon lithography of nanorods in su-8 photoresist*. Nanotechnology, vol. 16, no. 6, p. 846, 2005.
- [10] Torgersen, J.: *Novel biocompatible materials for in vivo two -photon polymerisation*. Ph.D. thesis, TU Wien, 4 2013.
- [11] Scanlab: *The RTC4 PC Interface Board for Real Time Control of Scan Heads and Lasers*, 2012.
- [12] Pawley, J.: *Handbook of Biological Confocal Microscopy*. 3rd Ed., Springer, 2006.
- [13] Zipfel, W.R., Williams, R.M. and Webb, W.W.: *Nonlinear magic: multiphoton microscopy in the biosciences*. Nat. Biotech, vol. 11, p. 1368–1376, 2003.
- [14] Ovsianikov, A., Shizhou, X., Farsari, M., Vamvakaki, M., Fotakis, C. and Chichkov, B.N.: *Shrinkage of microstructures produced by two-photon polymerization of zr-based hybrid photosensitive materials*. Opt. Express, vol. 17, no. 4, pp. 2143–2148, Feb 2009.
- [15] Ovsianikov, A., Viertl, J., Chichkov, B., Oubaha, M., MacCraith, B., Sakellari, I., Giakoumaki, A., Gray, D., Vamvakaki, M., Farsari, M. and Fotakis, C.: *Ultra-Low Shrinkage Hybrid Photosensitive Material for Two-Photon Polymerization Microfabrication*. ACS Nano, vol. 2, no. 11, pp. 2257–2262, November 2008.

- [16] Hell, S., Reiner, G., Cremer, C., and Stelzer, E.H.K.: *Aberrations in confocal fluorescence microscopy induced by mismatches in refractive index.*, Journal of Microscopy, vol.169, pt. 3, pp. 391-405, March 1993
- [17] Hitachi Launches World's Highest Resolution FE-SEM. *Nanotech Now*. 31 May 2011.
- [18] Aufreiter, M.: *Herstellung von CAD-basierenden Mikro-Partikeln mittels Zwei-Photonen Polymerisation*, Bachelor thesis, TU Wien, 2014
- [19] X.H. Qin, Z. Li, A. Ovsianikov, J. Torgersen, S. Mühleder, W. Holnthoner, J. Stampfl, R. Liska: *"Developing biodegradable 3D hydrogel scaffolds: from synthesis to two-photon polymerisation"*; Poster: European Symposium of Photopolymer Science ESPS 2012, Torino; 2012-09-04 - 2012-09-07; in: "European Symposium of Photopolymer Science - Book of Abstracts", (2012), 19.
- [20] A. Ovsianikov, M. Malinauskas, S. Schlie, B. Chichkov, S. Gittard, R. Narayan, M. Löbner, K. Sternberg, K.-P. Schmitz, and A. Haverich, *"Three-dimensional laser micro- and nano structuring of acrylated poly(ethylene glycol) materials and evaluation of their cytotoxicity for tissue engineering applications,"* Acta Biomater., vol. 7, no. 3, pp. 967–974, Mar. 2011.
- [21] A. Ovsianikov, A. Gaidukeviciute, B. N. Chichkov, M. Oubaha, B. D. MacCraith, I. Sakellari, A. Giakoumaki, D. Gray, M. Vamvakaki, M. Farsari, and C. Fotakis, *Two-Photon Polymerization of Hybrid Sol-Gel Materials for Photonics Applications*, Laser Chemistry, Article ID 493059, Volume 2008
- [22] Cargille, John J. *"Immersion oil and the microscope"*, 2nd ed. 1985
- [23] J. Serbin, A. Egbert, A. Ostendorf, B. N. Chichkov, R. Houbertz, G. Domann, J. Schulz, C. Cronauer, L. Fröhlich, and M. Popall, *"Femtosecond laser-induced two-photon polymerization of inorganic organic hybrid materials for applications in photonics,"* Opt. Lett., vol. 28, no. 5, p. 301, Mar. 2003.
- [24] Scanlab: *The RTC4 PC Interface Board for Real Time Control of Scan Heads and Lasers*, 2012.
- [25] J. R. Jones, O. Tsigkou, E. E. Coates, M. M. Stevens, J. M. Polak, and L. L. Hench, *"Extracellular matrix formation and mineralization on a phosphate-free porous bioactive glass scaffold using primary human osteoblast (HOB) cells,"* Biomaterials, vol. 28, no. 9, pp. 1653–1663, Mar. 2007.
- [26] W. Steiger, P. Gruber, A. Ajami, W. Husinsky, J. Stampfl, R. Liska, A. Ovsianikov, *Effect of the photoinitiator concentration on the spatial resolution of the two-photon polymerization*, micromachines, ISSN 2072-666X, 2014
- [27] Gebhardt, A.: *Generative Fertigungsverfahren*, Hanser Gardner Publications (2013).
- [28] Scanlab: Data sheet intelliSCAN®, January 2015, Available at: http://www.scanlab.de/de/-/Produkte/2D_Scan-Systeme/intelliSCAN#21039

8 TABLE OF FIGURES

Figure 1 Process chain of an additive manufacturing technology.....	1
Figure 2 (a) A free radical is formed and reacts with the monomer. (b) Those monomer molecules combine to large, fast growing chains. (c) Termination through combination: Two radicals combine and propagation is stopped. [3].....	4
Figure 3 Schemes of two different additive manufacturing technologies; (a) Stereolithography apparatus (SLA); a bottom-up system with scanning laser; (b) a top-down setup with digital light projection (DLP) modified from [4].....	6
Figure 4 Left picture: Jablonski diagram; $h\nu_{IR1}$ and $h\nu_{IR2}$: first and second photon absorbed in NIR spectral range; $h\nu_{UV}$: photon in UV spectral range; $h\nu_{vis}$: photon emitted in visible range; R^* : radical; T_1 : Triplet state; Right picture: Example of one- and two-photon excitation of fluorescence. [10]	7
Figure 5 (a) Polymerization takes part inside the material since 2PP is only limited to the focal point of the microscope, (b) 1PP/STL is limited to the surface of the material and therefore requires a layer-by-layer printing [19]	8
Figure 6 Dependence of the polymerized volume on the laser intensity in 2PP with the polymerization threshold and the threshold for polymer destruction [2].....	8
Figure 7 LSCM beam path.....	10
Figure 8 High NA microscope objective [6]	11
Figure 9 2PP-system [18]	13
Figure 10 Chemical structures of the reagents leading to the formation of an inorganic matrix during the sol-gel process [15].....	18
Figure 11 Colours of the hybrid materials with different PI-concentrations directly after application (small pictures) and after 4 hours of drying	19
Figure 12 Scheme of the sample mounting.....	21
Figure 13 Symbols used and their description.....	24
Figure 14 Different delays and their effects [24].....	26
Figure 15 Neubauer-improved hemocytometer.....	27
Figure 16 L929 mouse cells with F-actin stain (left) and F-actin + nucleus stain (right).....	28
Figure 17 Sol A 1%; 1x1 μ m cubes; monomer not sufficiently washed out	30
Figure 18 Sol A 1%; 5x5 μ m cubic particles with stems after 2 days in 2-propanol.....	30
Figure 19 Sol A 1%; 5 μ m cubes on glass substrate. When structuring too close to the surface of the glass slide the particles tend to stick to the surface which then results in partly great losses.....	31
Figure 20 Sol A 1%; 5 μ m cubes in 40 μ m filter	31
Figure 21 Sol A 1%; 5 μ m cubes in PBS. The remaining monomer was not washed out properly. This resulted in precipitation of salts when mixed with PBS.....	32
Figure 22 Sol D 0.1%; Arrays of 5x5 μ m cubes written with different speed at a power of 60mW each.....	33
Figure 23 Sol A 1%; arrays of cubes written with 40mm/s; 40-80mW	34
Figure 24 Sol A 1% (left) and Sol D 1% (right); Array of 5 μ m cubic particles, written with 50mW.....	34

Figure 25 Sol G 1%; partly burned and deformed array of 5 μ m cubic particles, written with 60mW.....	35
Figure 26 Sol A 0.1% TU-Logo of 10 μ m; 10-80mW, 20-29mm/s.....	36
Figure 27 Sol A 0.1%; TU-Logo 10 μ m (left) and 5 μ m (right); Power 10-100mW and Speed 20—50mm/s (+10mW per column, +3mm/s per row)	36
Figure 28 Sol A 0.1%; TU-Logo 5 μ m; Speed 10-100mm/s and power 10-100mW	37
Figure 29 Line test for (s) Sol D 0.1%, (b) Sol D 0.05%	38
Figure 30 Sol D 1%; Line test.....	38
Figure 31 Line test for (a) Sol A 1% (b) Sol F 1%.....	38
Figure 32 Sol A 1%; remainder of particles on a coverslip; pyramids with a 5x5 μ m base.....	39
Figure 33 Sol A 0.05%; pyramids of different sizes on a foundation; size of the base from left to right: 5x5 μ m, 4x4 μ m, 3x3 μ m, 2x2 μ m, 1x1 μ m, 0.5x0.5 μ m	40
Figure 34 Sol D 1%; Free standing lines; 65-100mW; Hatch in X- and Y-direction	40
Figure 35 Sol A 1%; (a) 5x5 μ m cubes with a hatch of 0.3 μ m and 0.1 dZ; magnification 63x, (b) SEM-image of arrays of 1x1x1 μ m cubes with a hatch of 0.1 μ m and 0.1 dZ.....	41
Figure 36 Sol D 1%; (a) arrays of 5 μ m cubes in 2-propanol after developing, magnification 20x (b) after sonification, magnification 40x (c) STL-file of cube-array.....	41
Figure 37 E 0.1%; (a) arrays of 1.25 μ m cubes in 2-propanol after developing; magnification 10x, (b) magnification 40x, (c) arrays of 1.25 μ m cubes after ultrasonication	42
Figure 38 Sol E 0.1%; 50 μ m stems, 30-100mW.....	43
Figure 39 Sol C 0.1%; Cubic particles with 50 μ m long stems and small foundations to improve adhesion; the particles form clusters in the middle.....	43
Figure 40 Sol A 0.1%; (a) Cubic particles on stems with different profiles, written at 90mW; stem-profiles from left to right: 1) \circ with diameter 1.5 μ m, stem length 50, 40, 30 μ m 2) \square with side length 1.5 μ m, stem length 50, 40, 30 μ m 3) Δ with side length 1.5 μ m. stem length 50, 40, 30 μ m 4, 5, 6) profiles like shown in (c), stem length 40, 50, 50 μ m, (b) stems with triangular profile and different length.....	44
Figure 41 Sol A 0.1%; particles with different stem-parameters; 70-90mW (left) and 80mW (right) (0,7x30) with 5 μ m cubes	44
Figure 42 Sol A 0.1%; particles with different stem-parameters; 70-90mW (left) and 70mW (right) (0,5x50) with 3 μ m cubes	45
Figure 43 Sol A 0.1%; particles with stems with quadratic (left) and round (right) profiles and a size of 1.5 μ m	45
Figure 44 Sol A 0.1%; particles with 55 μ m long stems with a diameter of 0,2 μ m.....	46
Figure 45 Sol A 0.1%; (a) from below: 5 μ m cubes with 17 μ m distance; 3 μ m cubes with 17 μ m, 7 μ m and 5 μ m distance between the cubes, (b) LSM image of the 3 rd and 4 th row (7 and 5 μ m distance), magnification 63x.....	46
Figure 46 Sol B 0.1%; LSM picture of stem particles in PBS; due to wrong correction factor the assembly of the single layers is incorrect and the structures appear distorted; the actual length of the stems is 20 μ m, the particles are cubes of 3 μ m	47
Figure 47 Sol A 0.1%; 5x5 μ m cubes on stems after 50 days in PBS	48
Figure 48 Survival of cells (L929, mouse cell line) on the different hybrid materials Sol A-G with 1%BIS.....	48

Figure 49 Sol E 0.1%; particles with stems seeded with cells (L929); Due to incorrect correction factor the indication of size is inaccurate	49
Figure 50 Sol E 0.1%; particles seeded with cells (L929); Bigger cells seem to collect the particles or at least grow around them.....	50
Figure 51 Particles seeded with L929; life stain; when too many cells are seeded on the sample it is difficult to distinguish between particles and cell since the hybrid materials are auto fluorescent and glow in whatever color they are excited	50
Figure 52 D 0.1%; Particles with stems seeded with L929 mouse cell line; Due to deficient actin staining the red parts are not visible despite maximum laser power at 640 nm	51
Figure 53 L929 mouse cells on a spot without particles; A too high number of cells makes it impossible to make a statement about particular cells	52
Figure 54 Sol E 0.1%; 2x2 μ m cubes on stems seeded with L929 mouse cells; stained for F-actin and nucleus; Right image: sectional view of the cell	52
Figure 55 Sol B 0.1%; 2x2 μ m particles on 20 μ m stems (blue) fixed on a glass-bottom petri dish and seeded with cells (L929, red); Staining: Actin (red) and nucleus (blue).....	53
Figure 56 Sol B 0.1%; 2x2 μ m particles on 20 μ m stems (blue) fixed on a glass-bottom petri dish and seeded with cells (L929, red); Staining: Actin (red) and nucleus (blue).....	54
Figure 57 Sol B 0.1%; 2x2 μ m particles on 20 μ m stems (blue) fixed on a glass-bottom petri dish and seeded with cells (L929, red); Staining: Actin (red) and nucleus (blue).....	54
Figure 58 (a) MC3T3 cells with 1 μ m cubic particles (Sol B 0.1%), (b) Sol A 0.1% particles with stems, seeded with MC3T3 cells; actin stain is not intense enough to be visible	55

9 LIST OF TABLES

Tab. 1 Sol-gel materials	17
Tab. 2 Different PI-concentrations used for experiments in this work.....	19
Tab. 3 Parameters of different objectives	20
Tab. 4 Refractive indices of the different hybrid materials.....	21
Tab. 5 Optimal and maximal writing speed for different objectives (focal lengths) [28]	23
Tab. 6 Average power for good structuring results for different PI-concentration.....	35
Tab. 7 LSM settings.....	50
Tab. 8 LSM settings.....	51
Tab. 9 LSM settings.....	53